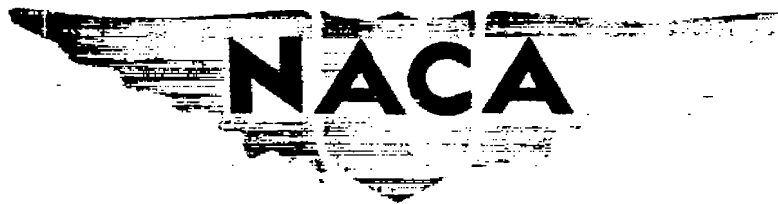


OCT 6 1948

Copy 2



RESEARCH MEMORANDUM

INVESTIGATION OF PERFORMANCE OF SINGLE-STAGE AXIAL-FLOW
COMPRESSOR USING NACA 5509-34 BLADE SECTION

By Harry Mankuta and Donald C. Guentert

Lewis Flight Propulsion Laboratory
Cleveland, Ohio



**NATIONAL ADVISORY COMMITTEE
FOR AERONAUTICS**

WASHINGTON
September 30, 1948

N A C A LIBRARY

LANGLEY MEMORIAL AERONAUTICAL
LABORATORY
Langley Field, Va.

NATIONAL ADVISORY COMMITTEE FOR AERONAUTICS

RESEARCH MEMORANDUM

INVESTIGATION OF PERFORMANCE OF SINGLE-STAGE AXIAL-FLOW

COMPRESSOR USING NACA 5509-34 BLADE SECTION

By **Harry Mankuta and Donald C. Guentert**

SUMMARY

An investigation was conducted to study the performance of a single-stage axial-flow compressor using blades with an NACA 5509-34 airfoil section. The compressor had a 14-inch tip diameter with a hub-to-tip diameter ratio of 0.8 at the entrance to the rotor. Static- and total-pressure, total-temperature, and flow-angle surveys were taken in the compressor inlet and outlet and between blade rows to study both the over-all performance and individual blade-row performance.

The performance of the rotor and stator blade rows is presented separately on the basis of three different measures of blade loading: turning angle, lift coefficient, and a loading factor defined as the ratio of the change in tangential velocity through the blades to the mean axial velocity. Discrepancies between the weight flow as measured by the orifice and the weight flow obtained by a mechanical integration of the axial-flow components across the passage at the various measuring stations indicated a need for more complete and precise instrumentation between the blade rows.

The over-all performance results at design speed showed that a maximum total-pressure ratio of 1.262 and a maximum adiabatic efficiency of 0.84 were obtained at an equivalent weight flow of 10.50 pounds per second.

INTRODUCTION

Axial-flow compressor research is currently aimed at obtaining information that will permit the design of axial-flow compressors with high pressure rise per stage without sacrifice of

efficiency or flow capacity. **One** phase of the research program is the development and investigation of various airfoil sections in two-dimensional and three-dimensional **cascades** for the purpose of obtaining information concerning blade loading and its limitations. Information of this nature is essential in the design of compressors that are to operate with a maximum pressure **rise** and high efficiency. Because of radial pressure gradients and flows set up by centrifugal forces, however, and because of the possible effects due to adjacent blade **rows, the** flow in an actual compressor is much more complex than that encountered in cascade investigations. Blade performance **must** therefore be investigated under actual compressor operating conditions in order to determine the effect of these additional variables. Because of the **complexities introduced** in the investigation of a multistage **compressor**, it is desirable to perform the investigation on a single-stage compressor consisting of an initial set of guide vanes followed by a set of rotor and a set of **stator** blades.

A 14-inch-diameter compressor of this type has been used at the **NACA** Cleveland laboratory to investigate the effect of different blade sections on compressor performance. The **hub-to-tip** diameter ratio of this compressor was 0.8 in order to be representative of the usual dimensions of the **middle** stages of a multistage compressor. The first set of blades investigated in this unit used the **NACA** 5509-34 airfoil section and was **similar** to the blades used **in** the fourth stage of the **NACA eight-stage** compressor (reference 1). A design procedure similar to that of reference 1, **which** had the **same** solidity and Mach number limitations, was used..

In order to obtain complete information concerning **flow** characteristics and individual blade-row performance in a single-stage **compressor**, **it is necessary to take pressure and temperature measurements** between the blade rows. Because of the very limited space available between the blade **rows**, difficulty was encountered **in** obtaining **instruments** sufficiently small to fit between the blade rows without sacrificing accuracy. In addition, the proximity of adjacent blade rows to **the** measuring plane very probably has an effect upon the pressure and angle measurements. Radial flows and pressure gradients also complicate the instrumentation. The problem of **instrumentation** was therefore important in the investigation of the **first blade** design.

This investigation was conducted over a wide range of air flows at corrected rotor speeds of 7265, **11,500**, and 14,530 **rpm**, corresponding to approximately **one-half**, three-quarters, and **full** design speed, **respectively**. The over-all **performance** is presented

as plots of total-pressure ratio **and** adiabatic efficiency **against** corrected weight flow. The individual blade-row **performance** is studied on the basis of three loading parameters: turning **angle**, lift coefficient, **and** a loading factor defined **as** the ratio **of** the change in tangential velocity **through** the blades to the **mean** axial velocity.

SYMBOLS

The following symbols are used in this report:

C_L	'liftcoefficient
c_p	specific heat at constant pressure, Btu/(lb)(°F)
g	acceleration due to gravity, 32.174, (ft/sec ²)
H_{ad}	adiabatio work input per pound, (ft-lb/lb)
a	actualworkinput per pound calculated from increase in angular momentum across rotor, (ft-lb/lb)
H_T	actual work input per pound calculated from total-temperature rise, (ft-lb/lb)
J	mechanical equivalent of heat, 778, (ft-lb/Btu)
K	constant in turning-angle relation
N	rotor speed, (rpm)
$N/\sqrt{\theta}$	rotor speed correctedto standardsea-level temperature, (rpm)
P	total pressure, (lb/sq ft absolute)
p	static pressure, (lb/sq ft absolute)
r	radius to blade element, (ft)
T	total temperature, (°R)
t	static temperature, (°R)
U	velocity of blade ωr at radius r , (ft/sec)

V	absolute afr velocity, (ft/sec)
V'	air velocity relative to rotor, (ft/sec)
W	weight flow rate, (lb/sec)
$W\sqrt{\theta/\delta}$	weight flow rate corrected to standard sea-level pressure and temperature, (lb/sec)
α	angle of attack , (deg)
α_0	angle of attack of isolated airfoil for zero lift , (deg)
β	absolute stagger angle, angle between compreeeor axis and absolute air velocity, (deg)
β'	relative stagger angle, angle between compressor axis and sir velocity relative to rotor, (deg)
γ	ratio of specific heats (c_p/c_v)
$\Delta\beta$	turning angle (stator), (deg)
$\Delta\beta'$	turning angle (rotor), (deg)
δ	ratio of inlet total pressure to standard sea-level pressure
η_{ad}	adiabatic efficiency of compreeeor
θ	ratio of inlet total temperature to standard sea-level temperature
ρ	density, (slugs/cu ft)
σ	blade-element solidity, ratio of chord length to distance between adjacent blades
ω	absolute angular velooity of blade, (radians/sec)

Subscripts:

0	inlet depression tank
1	inlet to rotor
2	inlet to stator

3	outlet of stator
av	average
e	referred to equivalent constant axial-velocity diagram
h	hub
m	referred to vector-mean velocity
t	tip
z	axial
e	tangential

COMPRESSOR DESIGN

Aerodynamic. - The first blade design to be investigated in the **14-inch variable-component** axial-flow compressor rig was design with a radial distribution of **velocity and pressure, aerodynamic limitation**, and flow **assumptions that were similar to** those used in the design of the fourth stage of the **NACA** eight-stage compressor (reference 1).

In this design procedure, 8 design velocity **diagram was** set up in which the **velocities** were expressed as ratios of the tip speed. In setting up this diagram, the following **conditions** were assumed:

1. Constant tip **diameter**
2. Ratio of hub-to-tip diameter at inlet to rotor blades equal to 0.8
3. Ratio of axial velocity **at hub** to **tip speed at** inlet to rotor **equal** to 0.6 (selected to provide **maximum** power input for hub-to-tip ratio of 0.6)
4. Vortex-type rotation added by rotor blades; **value** of change in tangential component **at hub** set by **OC_L limitation** cf 0.77; **rotation** added by **rotor** blades removed by **stator** blades
5. Symmetrical diagram at hub of rotor

6. Wheel-type rotation added by inlet guide vanes; value of tangential component added by -guide vanes at hub determined by **requirement** of **symmetrical** diagram
7. Constant total **enthalpy** and no radial component of flow assumed in **calculating** variation of **axial** velocity across passage entering and leaving each blade row; **value** of **axial velocity** component entering **stator** blades at hub determined by setting **Mach number** at hub on **stator** blades equal to Mach number at hub on preceding rotor **blades**
8. Passage height at each station determined by continuity requirement, with **compression process** assumed to be isentropic

Actual **velocities** were obtained by setting the Mach number of the maximum air **velocity** relative to the blades **equal** to 0.7.

Cascade **data** were **unavailable** on the NACA 5509-34 airfoil. The following relation, taken **from** reference 2, was therefore used to determine the **blade-angle settings** necessary to produce the required turning angles.

$$\theta = K(\alpha - \alpha_0)$$

The value of **K** was **taken** as 0.9, and **8 value** of -5.6' obtained **from** interpolation of isolated-airfoil tests, was used for the **angle** of **attack** at **zero** lift α_0 .

The NACA 5509-34 blade **section** was used for both **rotor and stator blades, which** were of **constant** section across the passage. The **coordinates** of the NACA 5509-34 blade **section are** presented in **table I**. The guide **vanes** were formed with circular **arc** surfaces **faired into** an elliptical nose section. Information concerning design turning angles and angles of **attack** for this blade design are given in the following table:

Blade row	Radius (in.)	Design stagger angle (deg)	Design turning angle (deg)	Design angle of attack (deg)
Guide vanes: 40 blades	Tip - 7.00	0	31.61	-----
	s - 6.82	0	30.45	-----
	b - 6.47	0	28.36	-----
	c - 6.11	0	26.33	-----
	d - 5.76	0	24.43	-----
	Hub - 5.60 (rotor leading edge)	0	23.58	-----
NACA 5509-34 airfoil section: rotor; 29 blades	Tip - 7.00	51.71	9.36	4.86
	s - 6.82	50.45	10.44	6.00
	b - 6.47	48.01	12.56	8.38
	c - 6.11	45.50	14.75	10.80
	d - 5.76	43.04	16.87	13.17
	Hub - 5.60 (rotor leading edge)	41.93	17.85	14.25
NACA 5509-34 airfoil section: stator; 30 blades	Tip - 7.00	47.81	17.25	13.66
	a - 6.84	46.75	17.04	13.32
	b - 6.51	44.87	16.72	13.03
	c - 6.18	43.21	16.60	12.91
	d - 5.85	41.81	16.71	13.00
	Hub - 5.70 (stator leading edge)	41.21	16.85	13.12

Mechanical. - The **mechanical** features of the compressor **are** shown in **figure 1**. The compressor had a constant tip diameter of 14.00 inches and 8 hub diameter that varied **from 11.20 inches** at the leading edge of the rotor blade to **11.72 inches** at the trailing edge of the **stator** blade. The axial **distance** between the trailing edge of one set of blades and the **leading** edge of the following set **was approximately 0.5 inch**. The clearance between the rotor-blade tips and the **compressor casing was 0.020 inch, whereas, the** clearance between the **stator** blades and the compressor hub **was 0.010 inch**. Three **spherically** seated journal bearings and a fixed-wedge-type thrust bearing were used on the rotor shaft. A set of exit turning vanes was located approximately 7 chord lengths downstream of the **stator** blades. These **turning vanes** were **designed** to remove the **remaining whirl** component of the air

with its resulting radial pressure gradient before **discharge** into the collector. **An annular baffle** was provided in the collector to aid in providing **uniform** flow around its **periphery**.

APPARATUS AND METHODS

Apparatus

A **sketch** of the **compressor** setup is shown in figure 2. Two **225-horsepower dynamometers** mounted in **tandem** were used to drive the **compressor** through a **7.25:1 speed increaser**. Air was taken in directly from the room through **8 thin-plate orifice** mounted in an **orifice tank** and then **passed** through **8 motor-operated throttle valve** into a large depression tank. This **tank** was 4 feet in diameter, 6 feet long, and contained **8 felt filter** and a **3-by-3-inch honey-comb** to aid in producing **smooth** flow at the **compressor** inlet. The tank sufficiently **reduced** the inlet-air velocities that the **compressor-inlet pressure and temperature** measurements made in the **tank** could be assumed to be **stagnation values**. A **bellmouth** inlet was used to provide a smooth flow from the tank into the compressor-inlet guide vanes. The compressor-discharge **collector** was connected to the laboratory **exhaust** system through two **exhaust** pipes. A motor-driven throttle valve was provided in the exhaust system to vary the **flow** through the compressor.

Instrumentation

Instrumentation was provided at the compressor inlet and outlet to measure over-all **compressor performance** and between **blade rows** to **measure** individual blade-row **performance**. The four instrument **stations** are shown in figure 1. **All** measurements at stations 1, 2, and 3 were taken at four **radial** positions **across** the **flow** passage. **All** instruments were **circumferentially** located in **such a manner** so to be removed **from** the wakes of upstream blades or **instruments**.

Station 0 was located in the inlet depression tank. **Because** of the size of this tank, the small existing velocities were neglected, and pressure and temperature measurements were **assumed** to be stagnation values. Temperatures in the inlet depression tank were **measured** by **four thermocouple probes**, each containing four thermocouples. **Two wall pressure** taps were **used** for pressure measurement.

Stations 1 and 2 were located approximately $1/5$ chord length before and after the rotor, respectively. **The total temperature** was

assumed to be constant across the **guide** vanes **and** across the **stator** blades, so no **temperatures** were measured at stations 1 and 2. Total pressures at each station were **obtained** with 8 single total-pressure rake similar to that shown in **figure 3(a)**. The variation in flow angle **from** hub to tip at a given flow was **considered** to be sufficiently small to **permit** the **orientation** of the rake in the direction **of the** flow in the center of the passage with negligible effect on the accuracy of the total-pressure measurements **at** the other radial positions. Because of the limited space existing between the blade rows, a special type of miniature static-pressure survey tube (fig. 3(b)) **was** designed. These tubes **were** individually calibrated with respect to **Mach** number. A single radial static-pressure survey of four points was taken with one of these tubes at stations 1 and 2. The orientation of **all** static-pressure tubes with the flow **yaw** angle was **accomplished** by **balancing** the pressures obtained from separate static-pressure taps on each side of the instrument.

In addition, three **wall static taps** in the outside **wall** were used. Flow-angle measurements **at each** station were obtained from 8 single **radial** survey with a **claw** tube similar to that shown in **figure 3(c)**.

Compressor-outlet measurements **were** made at station 3, which was **located** approximately 1 chord length downstream of the **stator** blades. Total-temperature measurements were **obtained** from four rakes containing four probe thermocouples each (fig. 3(d)). **In** order to **permit** the measurement of the energy addition to the air by means of the rise in **total** temperature **across** the **compressor**, a high degree of accuracy in the measurement of the total-temperature rise is required. For this **reason**, the **thermocouples** in the rakes **at** station 3 were connected differentially with those at station 0 in such 8 manner **to measure a circumferentially averaged value of the temperature** rise across the compressor at each of the **four** radii located by the four probes on each **rake**. Total-pressure measurements were obtained **from** four **19-tube circumferential** total-pressure rakes (fig. 3(e)) distributed around the periphery of the compressor. Each of these **rakes** was **located** at 8 different radial position and was **connected** differentially to the inlet depression tank to give a measurement of the total-pressure rise across the compressor at each of four **radii**.

Static pressure **at station** 3 was obtained from a single **radial** survey taken with a **Prandtl** type static-pressure tube shown in **figure 3(f)**. **In** addition, three **wall** static-pressure taps were provided in both the outside and inside wall. Flow angles were obtained by means of a single radial survey with a claw tube similar to that used at stations 1 and 2.

Airflow through the compressor was measured by a standard thin-plate intake orifice mounted in an orifice tank. Compressor speed was measured within ± 10 rpm with a precision-type tachometer.

A summary of the instrumentation used in the investigation is presented in the following table:

Station	Radial measuring positions (in.)	Measurement	Instrument	Circumferential positions
station 0, Inlet tank	-----	Total pressure	Wall tap	2
		Total temperature	Thermocouple probe	4
Station 1, after guide vanes	a - 6.82 b - 6.47 c - 6.11 d - 5.76	Total pressure	Radial total-pressure rake	1
		Static pressure	Miniature static-pressure survey	1
			Wall tap, outside wall	3
		Yaw angle	Claw survey tube	1
Station 2, after rotor	a - 6.64 b - 6.51 c - 6.18 d - 5.85	Total pressure	Radial total-pressure rake	1
		Static pressure	Miniature static-pressure survey tube	1
			Wall tap, outside wall	3
		Yaw angle	Claw survey tube	1
station 3, after stator	a - 6.66 b - 6.57 c - 6.29 d - 6.00	Total pressure	Circumferential total-pressure rake	4
		Static pressure	Static-pressure survey tube	1
			Wall tap, inside wall	3
			Wall tap, outside wall	3
		Total temperature	Thermocouple rake	4
		Yaw angle	Claw survey tube	1

Accuracy of Measurements

994

Over-all performance measurements. - The accuracy with which the over-all performance of the **compressor** may be expressed in terms of total-pressure ratio **and** **adiabatic** efficiency depends primarily upon the accuracy of the total-pressure **measurements** at stations 0 and 3 and **upon** the **measurement** of the total-temperature rise between these two stations. The method used in measuring the total pressure at stations 0 **and** 3 permits **an** accuracy within **approximately ±1** percent of the **dynamic** head. In order to obtain the **total-temperature** rise across the compressor, 8 recovery **coefficient** based on an **average** calibration curve of 8 group of thermocouple probes **was** applied to the observed **temperature** readings. **Differences** between the recovery coefficient of individual thermocouples **and** the average calibration curve **due** to **small** differences in the construction may introduce 8 small error in the **temperature** readings. An oil coating from bearing-oil leakage into the air stream may also change the thermocouple recovery coefficient sufficiently to introduce **an** error in the **temperature** measurements. When these sources of errors **are** considered, it is estimated **that** the measurements of temperature rise across the **compressor** are accurate to within approximately **±3** percent of the **stagnation** temperature rise.

Blade-row-performance measurements. - The problem of obtaining **air-flow** measurements **between** the blade rows **was complicated** by space limitations. At the **closest** points, the space between blade rows, was **approximately 1/2 inch**, which **means that** the actual measurements were taken within less **than 1/4 chord length** of the blades. **This** space limitation not only necessitated the use of very small pressure tubes with their attendant difficulties, but **also** increased the possibility of an effect upon the **measurements** by the flow **disturbances** generated. by the blades.

As a check on the **accuracy** of this instrumentation, the weight flows obtained by integrating the quantity $2\pi\rho gV_z r dr$ across the passage **at** stations 1, 2, **and** 3 were **compared** with the weight flow measured by the orifice. The **percentage discrepancy** between the integrated weight flow **at** each station **and** the orifice measured weight flow **are** plotted as a function of weight flow in figure 4.

The variation in the error in integrated weight flow **at** station 1 with **changes in flow** for three **speeds** are presented in figure 4(a). At this station, **all** the integrated weight flows were **within ±4 percent** of the orifice measured flows. **No** definite relation seems to exist between the error in weight flow **and** the weight flow Q_s measured by the orifice.

The variation in the **error** in integrated weight flow at station 2 with changes in flow at the same three **speeds** are presented in figure 4(b). At this station, the integrated weight flows vary from about 4 percent above the orifice-measured weight flow to approximately 7 percent **below**.

The variation in the error in integrated weight flow at station 3 with changes in flow at the three speeds are presented in figure 4(c). At most points at this station, the integrated weight flow was higher than the orifice-measured weight flow. The error in weight flow varied from approximately 13 to approximately -3 percent. In **general**, the difference between the integrated weight flow **and** the orifice measured weight flow decreased with increasing weight **flow**.

Possible causes for the large discrepancies between integrated weight flows and the weight flow measured by the orifice may be **divided** into three general categories: (1) differences between the flow conditions prevailing in the compressor **and** the uniform flow existing in the tunnel in which the instruments were calibrated, which made the calibrations invalid, (2) existence of unmeasured radial-flow components, and (3) circumferential-flow variations that may invalidate the application of measurements made at a single circumferential position to the entire periphery of the compressor.

Calibrations of all **pressure-measuring instruments** were obtained **under uniform steady-flow conditions**. In the **compressor**, these ideal-flow conditions do not exist and the calibration therefore may not be entirely accurate. **Immediately** downstream of the rotor (station 2), a fluctuating flow due to the wakes produced by the **rotor blades undoubtedly** exists. Because the total-pressure instruments under fluctuating-flow conditions **measure** the root-mean-square value of the velocity fluctuation rather than the average **value**, an error is introduced. It is possible that these flow fluctuations will also **affect** the accuracy **of** the static-pressure measurements.

Another flow condition that **may** cause an error in the **static-pressure measurements** is the presence of radial components of flow. A sufficiently large **component** of flow across the short dimension of the static-pressure tubes **may** cause an appreciable error in the static-pressure measurement. The actual magnitude of this error is unknown, however, as no measurements were made of **flow** pitch angle (angle between the flow direction and the compressor axis in a plane through the axis and the measuring point). Another **error** tending to

994

cause a discrepancy between integrated weight flow and orifice measured weight flow is introduced by the presence of radial components of flow inasmuch as the velocities calculated from the pressure measurements were assumed to have no radial component. This error is small, however, as a pitch angle of 10° causes an approximate error of only 1.5 percent in the axial velocity.

Circumferential variations in flow may be either a periodic symmetrical variation produced by the pressure fields or wakes set up by the stationary blades, or an unsymmetrical variation around the periphery of the compressor. With the exception of the circumferential total-pressure rakes used at station 3, all flow-measurement surveys were made at a single circumferential position. An error is obviously introduced if the flow conditions at this point do not represent an average condition. Although this possible error could not be evaluated, it is probably a primary factor in producing the discrepancies between the integrated weight flows and the weight flow as measured by the orifice.

The magnitude of the discrepancies existing between the integrated weight flows at the various measuring stations and the weight flow measured by the orifice makes it apparent that any individual blade-row performance results must be treated with caution. If these discrepancies are to be reduced in future investigations, it appears that circumferential surveys of all flow measurements must be made in order to detect and account for circumferential-flow variations produced by individual blades. In addition, it is probably advisable to provide some means for detecting unsymmetrical flow variations that may exist around the compressor periphery. Some provision for the measurement of flow pitch angle also appears to be desirable.

Methods of Investigation

During the investigation, the absolute pressure in the inlet tank was maintained at 25 Inches of mercury by throttling through the inlet valve. The weight flow was varied in approximately equal increments by varying the compressor back pressure with the outlet throttle. Runs were made at corrected rotor speeds $N/\sqrt{\theta}$ of 7265, 11,500, and 14,530 rpm, corresponding to approximately one-half, three-quarters, and full design speed, respectively. The range of Reynolds numbers covered during the investigation, based on blade chord, was approximately 250,000 to 500,000, and the Mach number of the flow relative to the blades varied from approximately 0.2 to 0.76.

Methods of Rating

Total-pressure ratio. - The total-pressure ratio used in this investigation is the average **pressure ratio** that would be obtained with an **isentropic power input** to the measured total air **flow** equal to the actual **isentropic power input** integrated over the flow passage. It **is** calculated by means of a mechanical integration of the **following equation**

$$\left(\frac{P_3}{P_0}\right)_{av} = \frac{\int_{r_{h,3}}^{r_{t,3}} \left[\left(\frac{P_3}{P_0}\right) - 1 \right] \rho_3 V_{z,3} r dr}{\int_{r_{h,3}}^{r_{t,3}} \rho_3 V_{z,3} r dr} + 1 \quad \frac{\gamma}{\gamma-1}$$

Adiabatic efficiency. - The adiabatic efficiency **used** in evaluating the **compressor performance** is based **on** the total-temperature rise **across the compressor and** is defined by the equation

$$\eta_{ad} = \frac{H_{ad}}{H_T}$$

The adiabatic **work** input per **pound** of air is H_{ad} and **is** calculated **from the** equation

$$H_{ad} = J c_p T_0 \left[\left(\frac{P_3}{P_0}\right)_{av}^{\frac{\gamma-1}{\gamma}} - 1 \right]$$

The **actual work** input per **pound** of air, as measured by the total-temperature rise across the **compressor**, is H_T . It **is** obtained **from a** mechanical integration of the following equation:

$$H_T = \frac{Jc_p \int_{r_{h,3}}^{r_{t,3}} (T_3 - T_0) \rho_3 V_{z,3} r dr}{\int_{r_{h,3}}^{r_{t,3}} \rho_3 V_{z,3} r dr}$$

Another method that was available to calculate the actual work **input** involves the determination of the **change** in **angular** momentum of the **flow** across the rotor. This **quantity** can be obtained from the equation

$$H_M = \frac{g}{g} \left[\left(\frac{\int_{r_{h,2}}^{r_{t,2}} V_{\theta,2} \rho_2 V_{z,2} r^2 dr}{\int_{r_{h,2}}^{r_{t,2}} \rho_2 V_{z,2} r dr} \right) - \left(\frac{\int_{r_{h,1}}^{r_{t,1}} V_{\theta,1} \rho_1 V_{z,1} r^2 dr}{\int_{r_{h,1}}^{r_{t,1}} \rho_1 V_{z,1} r dr} \right) \right]$$

A comparison of the work input determined by this method with the work input calculated from the **total-temperature** rise is shown in figure 5. In most cases, H_M is lower than H_T . The maximum difference between the curves varies from approximately 22 percent at design speed to approximately 16 percent at one-half design speed.

Because of the previously noted discrepancies between the integrated weight flows using the flow measurements at the various measuring stations and the **orifice measured weight flows**, H_M was not considered to be as accurate as H_T . For this reason, the efficiencies were calculated on a total-temperature-rise basis.

RESULTS AND DISCUSSION

The data obtained at the three rotor speeds are presented in table II.

Over-all Performance

The over-all performance of the **compressor** is presented in figure 6 as curves of total-pressure ratio and adiabatic **temperature-rise efficiency** against equivalent weight flow.

At design speed, a peak total-pressure ratio of 1.262 was obtained at an efficiency of 0.64 **and** an equivalent weight flow of 10.50 pounds per second. Design value for the total-pressure ratio was 1.210 at an equivalent weight flow of 13.45 **pounds per second**, based on an isentropic compression process. Because of **restrictions** in the exhaust system, the **maximum** corrected weight flow obtained during the performance tests was 13.25 pounds **per second**. With an efficiency of 0.71 obtained by extrapolating the **efficiency curve** to the design weight flow, the design pressure ratio would be 1.146 as **compared** to an actual value of 1.140 obtained by extrapolating the pressure-ratio curve to the design weight flow.

The peak adiabatic temperature-rise efficiency at design speed **was** 0.84 and was obtained at approximately the same weight flow for which the maximum pressure ratio was obtained. The peak efficiency increased to 0.92 at one-half design speed (7265 **rpm**). These efficiencies were obtained with interstage instrumentation in place. Check runs made with this **instrumentation removed** showed an increase in efficiency varying between 1 and 3 percent over the upper **half** of the flow range at the three speeds.

When the absolute values of the adiabatic temperature-rise efficiency are considered, it should be **remembered** that these values are based on a power input **determined** from a **measurement** of the **total-temperature rise** across the **compressor**. **Because the temperature rise** across a single-stage axial-flow **compressor** is small, of the order of **magnitude** of the stagnation-temperature rise, a small error in the temperature measurement may introduce an appreciable **error** in the efficiency.

Blade-Row Performance

Pressure rise in a blade row is a function of turning imparted to the air, or blade loading. The performance of rotor **and stator**

blade rows is presented in figures 7 to 9 on the **basis** of three different measures of blade loading. In figures 7(a) and 7(b), a plot of turning angle against angle of attack is presented for the rotor **and stator**, respectively. For this plot, an **equivalent constant axial-velocity diagram**, (shown with dotted lines in fig. 10) was used to obtain values of turning angle and angle of attack. This method is the method used **in** reference 3 to obtain correlation between turning angles obtained in a variable axial-velocity three-dimensional cascade **and turning angles obtained in a constant axial-velocity two-dimensional cascade**.

Curves are plotted in **figures** 7 to 9 for four different radii at three speeds. The effect of speed on the **turning** angle appears to be very small. It **should be** noted that because the variation in angle of attack was **obtained** by varying the **flow, the air stagger angle** did not remain **constant**. Any effect of the **air stagger angle** on turning angle **will therefore** also appear **in** these curves. Reference 4 indicates that the value of **K** in the **expression $\theta = K(\alpha - \alpha_0)$** varies appreciably with changes in stagger angle and solidity.

The design point at each **radius** is also indicated. At the design angle of attack on the rotor, **the measured turning angle** at all radial positions except d were within 1° of the design turning angle predicted by the equation

$$\theta = 0.9 (\alpha - \alpha_0)$$

For the **stator** blades, the **design turning** angles were within 3° of **the** measured turning angles with the exception of the radial position near the hub where the **measured turning angle** was 7° lower than the **design value**.

Curves of σC_L **against an entering-air angle of attack based on** the velocity vectors V'_1 and V_2 (fig. 10) for the **rotor and stator** are plotted in figures 8(a) and 8(b), **respectively**. Drag forces were neglected **in** calculating the values of σC_L **and** the lift force was assumed to be **normal** to the mean relative **velocity vectors V'_m and V_m** for the rotor and the **stator**, respectively. The values of σC_L were calculated **from** the equations

$$\sigma C_L = \frac{2\Delta V'_\theta}{V'_m} \quad (\text{rotor})$$

$$\sigma C_L = \frac{2\Delta V_\theta}{V_m} \quad (\text{stator})$$

In figures 9(a) and 9(b) are plotted curves of a loading factor $\Delta v'_\theta/v'_{z,m}$ against $v'_{\theta,m}/v'_{z,m}$ for the rotor and of $\Delta v_\theta/v_{z,m}$ against $v_{\theta,m}/v_{z,m}$ for the stator.

SUMMARY OF RESULTS

As a result of the investigation conducted to study the performance of a single-stage axial-flow compressor using blades with an NACA 5509-34 airfoil section, the following results were obtained:

1. At design speed, a maximum total-pressure ratio of 1.262 and a maximum adiabatic efficiency of 0.84 were obtained at an equivalent weight flow of 10.50 pounds per second.

2. The measured turning angles across the rotor at all radial positions except near the hub were within 1° of the design turning angles at the design angles of attack. For the stator blades, the design turning angles were within 3° of the measured turning angles with the exception of the radial position near the hub where the measured turning angle was 7° lower than the design value.

Lewis Flight Propulsion Laboratory,
National Advisory Committee for Aeronautics,
Cleveland, Ohio.

REFERENCES

1. Sinnette, John T., Schey, Oscar W., and King, J. Austin: Performance of NACA Eight-Stage Axial-Flow Compressor Designed on the Basis of Airfoil Theory. NACA Rep. No. 758, 1944.
2. Kantrowitz, Arthur, and Daum, Fred L.: Preliminary Experimental Investigation of Airfoils in Cascade. NACA CB, July 1942.'
3. Bogdonoff, Seymour M., and Herrig, L. Joseph: Performance of Axial-Flow Fan and Compressor Blades Designed for High Loadings. NACA TN No. 1201, 1947.

4. **Bogdonoff, Seymour M.**, and **Hess, Eugene E.**: **Axial-Flow Fan and Compressor Blade Design Data at 52.5° Stagger and Further Verification of Cascade Data by Rotor Tests.** NACA TN Ho. 1271, 1947.

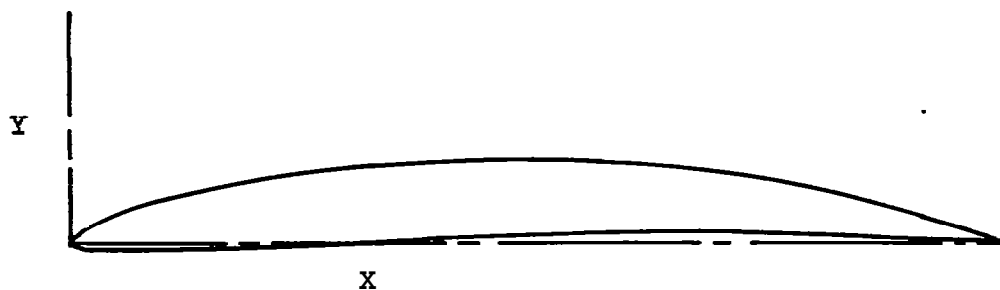
•

•

•

•

TABLE 1. -SECTION COORDINATES OF NACA 5509-34 BLADE SECTION



UPPER SURFACE		LOWER SURFACE	
X	Y	X	Y
0.00	0.00	0.00	0.00
1.03	1.23	1.47	-.41
2.21	1.96	2.79	-.49
4.64	3.13	5.36	-.54
7.10	4.11	7.90	-.52
9.58	4.94	10.42	-.47
14.58	6.36	15.42	-.33
19.61	7.45	20.39	-.15
29.73	8.95	30.27	.27
39.88	9.68	40.12	.69
50.04	9.76	49.96	1.02
60.19	9.23	59.81	1.26
70.30	8.05	69.70	1.35
80.38	6.13	79.62	1.20
90.28	3.31	89.72	.56
95.16	1.68	94.84	.18
100.00	.09	100.00	-.09



TABLE 11 - SUMMARY OF PERFORMANCE DATA OF 14-INCH SINGLE-STAGE AXIAL-FLOW COMPRESSOR USING NACA 6300-34 BLADE SECTION

		Station 0		Station 1						Station 2						Station 3									
Equivalent weight flow (orifice) W/W ₀ (lb/sec)	Radial position	Pressure p = P (in. Hg abs.)	Temperature t = T (°R)	Radius (in.)	Actual blade speed (ft/sec)	Total pressure P (in. Hg abs.)	Static pressure p (in. Hg abs.)	Total temperature, T (°R)	Flow angle β ₁ (deg)	Absolute air velocity (ft/sec)	Radius (in.)	Actual blade speed (ft/sec)	Total pressure P (in. Hg abs.)	Static pressure p (in. Hg abs.)	Total temperature, T (°R)	Flow angle β ₂ (deg)	Absolute air velocity (ft/sec)	Radius (in.)	Total pressure P (in. Hg abs.)	Static pressure p (in. Hg abs.)	Total temperature, T (°R)	Flow angle β ₃ (deg)	Absolute air velocity (ft/sec)		
Equivalent rotor speed, 14,530 rpm (design)																									
C	13.25	a	24.88	542.2	5.82	892.8	24.22	20.44	542.2	25.25	893.7	6.84	906.9	22.42	22.87	872.9	41.75	692.3	6.85	28.43	22.22	872.9	25.00	885.0	
		b			5.47	837.7	24.85	20.28		25.25	897.8	6.81	843.9	22.05	22.55	874.0	40.70	718.1		6.57	28.27	22.09	874.0	25.00	881.4
		c			5.11	792.6	24.85	20.18		24.20	818.0	6.18	802.0	22.46	22.46	871.9	39.85	794.5		6.29	28.25	21.95	871.9	23.50	878.9
	11.28	n	545.4	5.82	885.6	24.90	22.07	545.4	24.75	472.1	6.84	888.7	31.11	26.46	890.9	46.25	886.8	6.55	31.25	27.00	890.9	29.50	887.6		
				b	5.47	840.4	24.99		21.94	24.75	490.5	6.81	845.6	31.65	26.33	898.4	47.75	891.6	6.27	31.07	26.92	898.4	29.50	887.0	
				c	5.11	795.2	24.99		21.78	24.75	503.6	6.18	804.5	31.45	25.33	897.5	47.25	891.7	6.29	31.41	25.80	897.5	29.50	885.4	
	10.42	d	545.4	5.82	885.0	24.94	22.06	545.4	24.75	432.4	6.84	889.2	32.11	27.10	894.1	54.58	882.3	6.55	31.25	27.72	894.1	31.50	886.4		
				b	5.47	840.6	24.99		22.33	24.75	455.7	6.81	847.0	32.41	27.22	898.8	50.25	890.6	6.27	31.07	27.71	898.8	30.50	883.9	
				c	5.11	795.6	24.99		22.21	24.75	457.3	6.18	804.0	31.80	27.07	898.5	49.75	878.9	6.29	31.84	27.64	898.5	30.50	880.7	
	9.52	a	25.00	544.3	5.82	892.5	24.96	23.04	544.3	22.25	355.7	6.84	883.9	32.37	27.12	894.1	65.45	882.5	6.55	30.95	27.80	894.1	30.00	884.7	
					b	5.47	837.7	24.99		22.89	22.25	404.3	6.81	843.9	32.45	27.21	898.5	63.25	891.3	6.27	31.30	27.72	898.5	31.00	882.3
					c	5.11	795.6	24.99		22.75	24.20	415.8	6.18	804.0	33.52	27.22	898.1	60.75	894.8	6.29	31.59	27.52	898.1	29.50	884.6
8.72	b	25.00	543.1	5.82	883.0	24.95	23.42	543.1	24.75	343.9	6.84	887.0	32.15	26.87	895.4	72.75	889.9	6.55	30.46	27.72	895.4	29.50	889.1		
				b	5.47	838.5	24.97		23.25	24.75	363.3	6.81	845.0	32.06	26.99	891.9	68.25	892.5	6.27	30.74	27.55	891.9	30.50	886.4	
				c	5.11	793.6	24.99		23.12	24.25	378.9	6.18	803.0	32.55	27.00	899.5	60.95	897.6	6.29	31.18	27.46	899.5	30.50	882.6	
8.44	c	25.00	543.4	5.82	883.9	24.96	23.05	543.4	22.25	378.7	6.85	759.4	32.31	27.05	899.3	49.25	892.4	6.55	30.71	27.47	899.3	31.00	882.3		
				b	5.47	838.5	24.96		23.36	24.75	389.1	6.81	847.0	30.43	26.85	895.2	70.75	884.1	6.27	30.18	27.64	895.2	29.50	885.5	
				c	5.11	793.6	25.00		23.24	24.25	387.4	6.18	803.0	32.05	26.99	891.2	61.75	817.5	6.29	30.84	27.33	891.2	30.50	886.2	
8.10	d	25.00	542.4	5.82	883.9	24.95	23.70	542.4	21.75	373.0	6.85	759.4	32.43	26.85	899.0	49.25	893.7	6.55	30.47	27.34	899.0	30.50	884.6		
				b	5.47	838.5	24.96		23.50	24.75	398.2	6.84	887.0	30.82	26.85	895.9	74.25	848.2	6.27	30.01	27.58	895.9	29.50	886.0	
				c	5.11	793.6	25.00		23.35	24.25	390.7	6.18	803.0	33.65	26.81	899.5	61.25	828.8	6.29	30.78	27.33	899.5	31.25	887.4	
7.789	a	25.00	543.0	5.82	893.9	24.98	23.70	543.0	24.75	295.6	6.84	887.0	31.12	26.54	898.5	77.75	887.3	6.55	29.95	27.58	898.5	29.00	887.7		
				b	5.47	838.5	24.98		23.62	24.75	323.0	6.81	845.0	31.88	26.85	896.0	64.75	887.4	6.27	30.03	27.36	896.0	31.50	883.3	
				c	5.11	793.6	24.99		23.49	24.25	336.2	6.18	803.0	32.44	26.76	891.8	61.70	817.7	6.29	30.83	27.29	891.8	32.00	875.0	
	d		543.0	5.82	893.9	24.98	23.25	543.0	22.25	345.0	6.85	759.4	32.36	26.83	892.4	47.75	895.6	6.55	29.94	27.32	892.4	30.50	889.6		
				b	5.47	838.5	24.98		23.50	24.75	356.8	6.81	845.0	31.66	26.85	894.4	67.55	896.8	6.27	30.36	27.47	894.4	31.00	889.5	
				c	5.11	793.6	25.00		23.24	24.25	357.4	6.18	803.0	32.05	26.99	891.2	61.75	817.5	6.29	30.84	27.33	891.2	30.50	886.2	
Equivalent rotor speed, 11,800 rpm																									
11.63	a	25.00	543.9	5.82	700.2	24.83	21.88	543.9	23.25	484.4	6.84	702.7	26.46	22.82	857.5	35.75	551.9	6.55	26.27	21.82	857.5	29.50	886.1		
				b	5.47	654.4	24.87		21.72	24.25	506.8	6.81	659.4	27.11	22.24	867.4	35.40	608.3	6.27	25.81	21.78	857.4	29.00	882.6	
				c	5.11	628.7	24.88		21.71	24.75	526.3	6.18	635.1	27.32	22.06	867.7	35.25	600.0	6.29	25.99	21.66	857.7	23.50	884.3	
10.93	b	25.00	545.0	5.82	700.6	24.90	22.26	545.0	25.00	515.9	6.85	601.6	28.92	21.91	859.0	34.25	631.0	6.55	26.88	21.64	859.0	29.50	882.6		
				b	5.47	654.8	24.90		22.21	24.75	447.2	6.84	703.1	27.67	23.91	863.6	41.25	541.3	6.26	27.48	22.72	863.6	29.00	882.4	
				c	5.11	629.1	25.00		22.13	24.25	473.7	6.18	635.5	28.04	23.51	863.1	40.25	579.1	6.29	27.89	22.56	863.1	24.00	885.8	
10.32	c	25.00	544.2	5.82	700.2	24.90	22.67	544.2	22.70	473.7	6.85	601.6	27.63	23.81	863.1	38.75	559.1	6.55	27.14	22.44	863.1	29.50	882.1		
				b	5.47	654.4	24.98		22.65	24.25	418.1	6.84	702.7	28.23	24.80	866.4	43.75	615.7	6.26	28.05	24.70	866.4	27.00	884.0	
				c	5.11	628.7	24.99		22.47	24.25	442.8	6.18	635.1	28.38	24.43	866.1	42.45	585.6	6.29	28.25	24.85	866.1	25.00	881.4	
	d		543.0	5.82	700.2	24.90	22.37	543.0	22.75	452.9	6.85	601.6	28.05	24.19	866.2	40.75	532.5	6.55	27.21	24.48	866.2	31.00	881.9		
				b	5.47	654.4	24.98		22.65	24.25	433.8	6.81	645.0	28.40	24.43	866.1	42.75	642.4	6.27	28.27	24.67	866.1	27.00	881.6	
				c	5.11	628.7	24.99		22.47	24.25	442.8	6.18	635.1	28.38	24.43	866.1	42.45	585.6	6.29	28.25	24.85	866.1	25.00	881.4	
	d		543.0	5.82	700.2	24.90	22.37	543.0	22.75	452.9	6.85	601.6	28.05	24.19	866.2	40.75	532.5	6.55	27.21	24.48	866.2	31.00	881.9		

0.90	a	25.00	545.5	6.82	700.6	24.97	22.79	545.5	24.75	410.8	0.84	703.1	22.09	25.01	570.8	45.25	473.7	0.86	25.22	25.10	570.8	22.00	496.3
	b			6.47	654.8	24.99	22.45		25.25	423.5	0.81	699.9	22.09	24.80	570.7	44.25	538.0	0.87	25.25	25.03	570.7	22.00	511.1
	c			6.11	629.1	24.90	22.80		24.25	432.7	0.18	635.5	22.73	24.85	569.9	44.25	538.2	0.29	25.45	24.97	569.9	22.00	502.2
	d			5.75	592.1	24.85	22.49		19.75	423.5	0.82	691.9	22.89	24.85	559.2	42.75	527.9	0.00	27.85	24.99	559.2	22.00	473.1
0.95	a	25.00	545.0	6.82	700.2	24.99	23.43	545.0	23.75	337.5	0.84	702.7	22.11	25.40	559.7	45.45	443.8	0.85	25.57	25.51	559.7	22.00	457.9
	b			6.47	654.4	24.98	22.91		25.05	399.8	0.51	699.4	22.08	25.37	559.5	45.45	512.3	0.57	25.81	25.25	559.5	22.00	450.2
	c			6.11	628.7	24.95	25.79		23.75	412.1	0.18	635.1	22.80	25.20	558.0	44.75	505.7	0.29	25.65	25.00	558.0	22.00	455.4
	d			5.75	591.7	24.79	22.71		22.25	423.2	0.83	691.5	22.84	25.02	559.3	43.75	509.5	0.00	26.11	25.43	559.3	22.00	439.3
0.92	a	25.00	545.1	6.82	700.2	24.99	23.09	545.1	24.25	367.5	0.84	702.7	22.82	25.04	573.9	50.25	459.2	0.86	25.75	25.19	573.9	22.00	427.1
	b			6.47	654.4	24.98	23.14		24.75	378.4	0.51	699.4	22.13	25.69	571.8	47.45	477.8	0.57	26.02	25.13	571.8	22.00	452.1
	c			6.11	623.7	24.99	23.10		24.25	363.1	0.18	635.1	22.04	25.79	571.8	47.25	479.5	0.29	25.95	25.11	571.3	22.00	449.2
	d			5.75	591.7	24.82	23.05		22.75	374.0	0.85	691.5	22.06	25.71	572.9	45.25	495.9	0.00	25.65	25.02	572.9	22.00	432.2
0.88	a	25.00	545.4	6.82	700.2	24.91	23.89	545.4	24.75	321.4	0.84	702.7	22.07	25.19	575.1	52.75	443.8	0.85	25.91	25.09	575.1	22.00	395.1
	b			6.47	654.4	24.99	23.44		24.75	344.9	0.51	699.4	22.14	25.49	572.9	49.75	485.4	0.57	26.13	25.05	572.9	22.00	415.4
	c			6.11	625.7	24.99	23.41		24.25	347.5	0.18	635.1	22.23	26.20	572.4	48.75	453.7	0.29	26.14	25.55	572.4	22.00	422.3
	d			5.75	591.7	24.92	23.33		22.75	350.0	0.85	691.5	22.31	26.21	574.1	45.25	495.2	0.00	25.84	25.52	574.1	22.00	405.1
7.07	a	25.00	545.4	6.82	700.2	24.91	23.95	545.4	24.75	283.5	0.84	702.7	22.23	25.21	577.2	50.25	470.9	0.85	26.74	25.75	577.2	22.00	375.0
	b			6.47	654.4	24.99	23.80		24.75	301.7	0.51	699.4	22.44	26.19	572.8	51.25	475.4	0.57	26.03	25.71	572.8	22.00	403.5
	c			6.11	628.7	24.99	23.84		24.25	301.4	0.18	635.1	22.09	26.22	574.2	50.45	461.1	0.29	26.17	25.64	574.2	22.00	421.1
	d			5.75	591.7	24.82	23.54		22.75	305.0	0.85	691.5	22.26	26.22	574.5	49.25	484.3	0.00	25.95	25.51	574.5	22.00	405.3
7.03	a	25.00	545.2	6.82	700.2	24.92	24.03	545.2	24.25	280.7	0.84	702.7	22.57	25.00	578.0	70.75	455.5	0.85	25.45	25.74	578.0	22.00	350.0
	b			6.47	654.4	24.99	23.92		24.25	283.5	0.51	699.4	22.23	25.84	575.5	55.45	453.2	0.57	26.00	25.63	575.5	22.00	403.7
	c			6.11	628.7	24.99	23.81		24.25	285.5	0.18	635.1	22.73	25.04	575.0	51.75	456.5	0.29	25.95	25.59	575.0	22.00	410.7
	d			5.75	591.7	24.95	23.75		22.75	304.5	0.85	691.5	22.60	25.11	574.1	49.75	454.4	0.00	25.73	25.50	574.1	22.00	393.1

Equivalent rotor speed, 7,035 rpm

5.27	a	24.92	541.9	6.82	440.1	24.89	23.40	541.9	24.25	330.8	0.84	441.5	23.23	23.44	546.4	32.25	380.2	0.85	25.19	22.03	545.4	22.00	409.0
	b			6.47	417.5	24.90	23.37		24.75	341.7	0.51	420.7	23.51	23.25	547.0	32.75	405.9	0.57	25.43	22.03	547.0	22.00	434.7
	c			6.11	395.1	24.90	23.30		24.25	340.0	0.18	399.9	23.55	23.31	545.7	31.75	421.3	0.29	25.45	22.00	545.7	22.00	437.3
	d			5.75	371.9	24.85	23.25		22.25	345.5	0.85	379.1	23.42	23.25	547.2	32.25	406.8	0.00	25.40	22.95	547.2	22.00	434.0
7.41	a	25.01	543.0	6.82	441.7	24.95	23.55	543.0	24.25	292.3	0.84	443.3	23.09	24.30	550.0	30.75	345.9	0.85	25.37	24.11	550.0	22.00	363.5
	b			6.47	419.2	25.00	23.77		24.25	305.9	0.51	422.3	23.10	24.22	550.5	30.25	373.3	0.57	25.01	24.07	550.5	22.00	392.4
	c			6.11	395.5	25.00	23.74		24.25	300.5	0.18	401.3	23.14	24.19	549.9	37.95	358.0	0.29	25.05	24.09	549.9	22.00	364.4
	d			5.75	372.3	24.97	23.67		22.25	315.4	0.85	379.5	23.09	24.11	549.9	37.55	375.3	0.00	25.79	24.01	549.9	22.00	365.0
1.1	a	24.99	542.9	6.82	441.9	24.99	23.99	542.9	24.99	270.5	0.84	443.5	23.14	24.59	551.1	42.25	355.7	0.85	25.17	24.32	551.1	22.00	359.2
	b			6.47	419.4	24.99	23.93		24.25	282.9	0.51	422.5	23.53	24.59	551.9	42.25	352.0	0.57	25.27	24.51	551.9	22.00	352.0
	c			6.11	395.5	24.99	23.91		24.25	285.0	0.18	401.5	23.52	24.05	551.0	41.25	349.3	0.29	25.23	24.59	551.0	22.00	351.8
	d			5.75	373.7	24.92	23.87		22.25	295.0	0.85	379.7	23.19	24.57	551.0	40.25	346.7	0.00	25.03	24.53	551.0	22.00	334.0
0.36	a	24.99	543.8	6.82	442.4	24.91	24.11	543.8	24.25	243.1	0.84	444.0	23.23	24.69	553.4	44.50	303.9	0.85	25.40	25.05	553.4	22.00	315.7
	b			6.47	419.5	24.95	24.07		24.25	253.7	0.51	422.9	23.53	24.95	553.5	44.75	340.1	0.57	25.45	24.85	553.5	22.00	345.1
	c			6.11	397.2	24.99	24.04		23.25	257.1	0.18	401.9	23.49	24.90	552.0	43.95	342.0	0.29	25.42	24.95	552.0	22.00	320.8
	d			5.75	373.9	24.95	23.99		22.25	270.2	0.85	380.1	23.37	24.84	552.5	42.75	335.9	0.00	25.23	24.92	552.5	22.00	312.3
5.76	a	25.00	543.3	6.82	441.9	25.04	24.31	543.3	24.75	294.9	0.84	443.5	23.30	25.24	555.5	45.25	379.4	0.85	25.45	25.41	555.5	22.00	275.3
	b			6.47	419.4	24.99	24.26		24.25	294.0	0.51	422.5	23.53	25.30	553.4	45.75	360.9	0.57	25.05	25.23	553.4	22.00	292.0
	c			6.11	395.5	24.99	24.24		23.75	293.7	0.18	401.5	23.52	25.29	553.0	45.75	312.6	0.29	25.55	25.35	553.0	22.00	294.9
	d			5.75	373.5	24.97	24.19		22.25	245.2	0.85	379.7	23.59	25.29	552.8	45.25	307.1	0.00	25.45	25.30	552.8	22.00	292.0
5.01	a	25.00	543.5	6.82	441.9	24.91	24.47	543.5	24.25	182.4	0.84	443.5	23.59	25.53	555.5	55.75	279.9	0.85	25.55	25.56	555.5	22.00	252.4
	b			6.47	419.4	24.98	24.43		24.25	201.9	0.51	422.5	23.78	25.55	554.9	46.25	295.4	0.57	25.63	25.67	554.9	22.00	256.4
	c			6.11	395.5	24.98	24.43		23.25	214.5	0.18	401.5	23.77	25.52	554.5	46.25	301.2	0.29	25.65	25.67	554.5	22.00	250.2
	d			5.75	373.5	24.95	24.39		22.25	214.5	0.85	379.7	23.77	25.54	554.5	46.25	295.3	0.00	25.55	25.51	554.5	22.00	252.9
4.98	a	24.99	543.8	6.82	441.5	24.95	24.07	543.8	24.55	185.9	0.84	443.1	23.75	25.20	557.0	55.25	301.5	0.85	25.52	25.71	557.0	22.00	245.3
	b			6.47	419.5	24.95	24.05		24.55	182.5	0.51	422.1	23.78	25.51	556.9	51.75	301.5	0.57	25.57	25.55	556.9	22.00	250.0
	c			6.11	395.4	24.95	24.46		23.75	197.1	0.18	401.1	23.83	25.51	556.2	50.75	310.3	0.29	25.63	25.59	556.2	22.00	253.0
	d			5.75	373.1	24.98	24.44		22.25	201.5	0.85	379.3	23.82	25.52	556.2	50.25	307.5	0.00	25.50	25.59	556.2	22.00	250.3
4.36	a	25.00	543.5	6.82	441.9																		

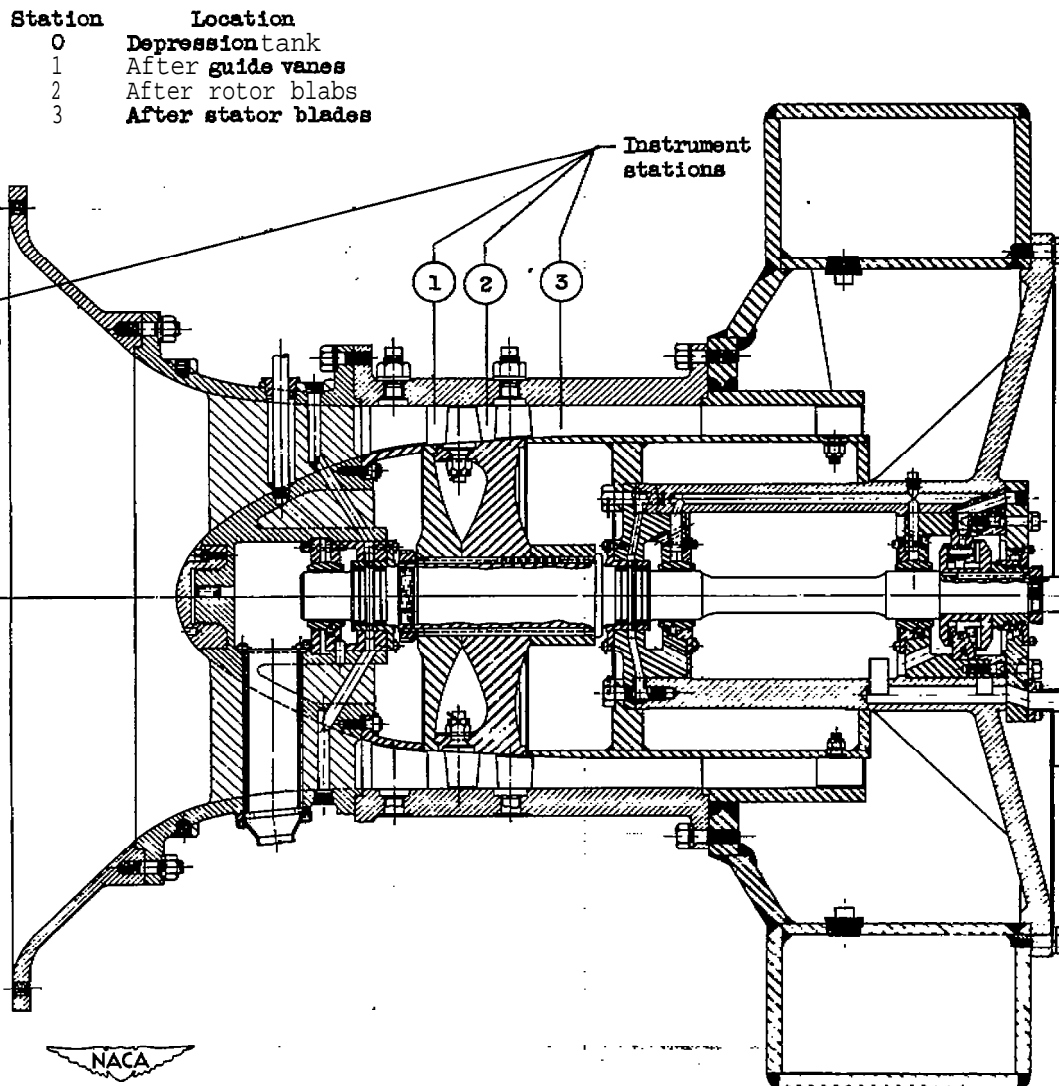


Figure 1. - Cross-sectional view of compressor showing instrument stations.

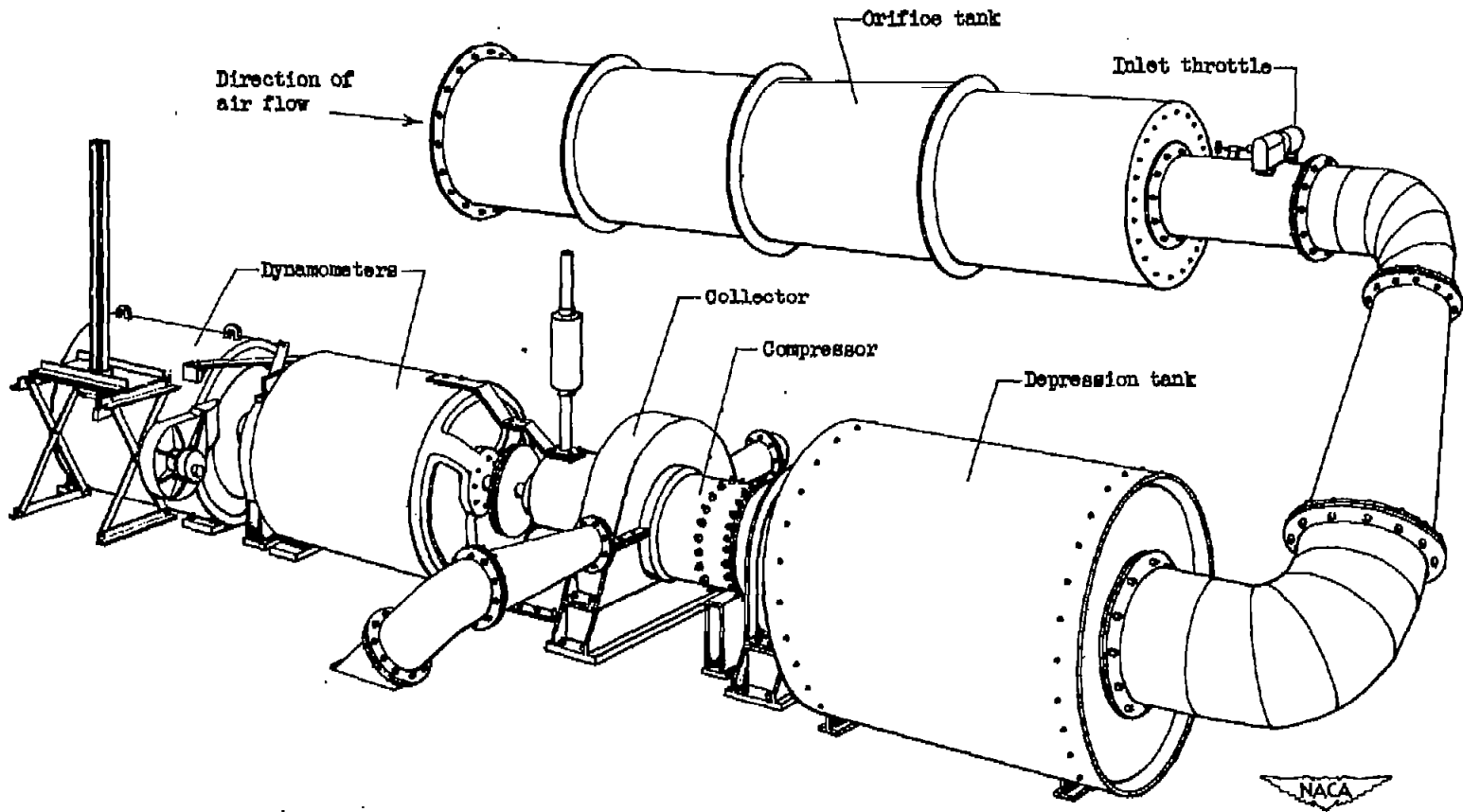
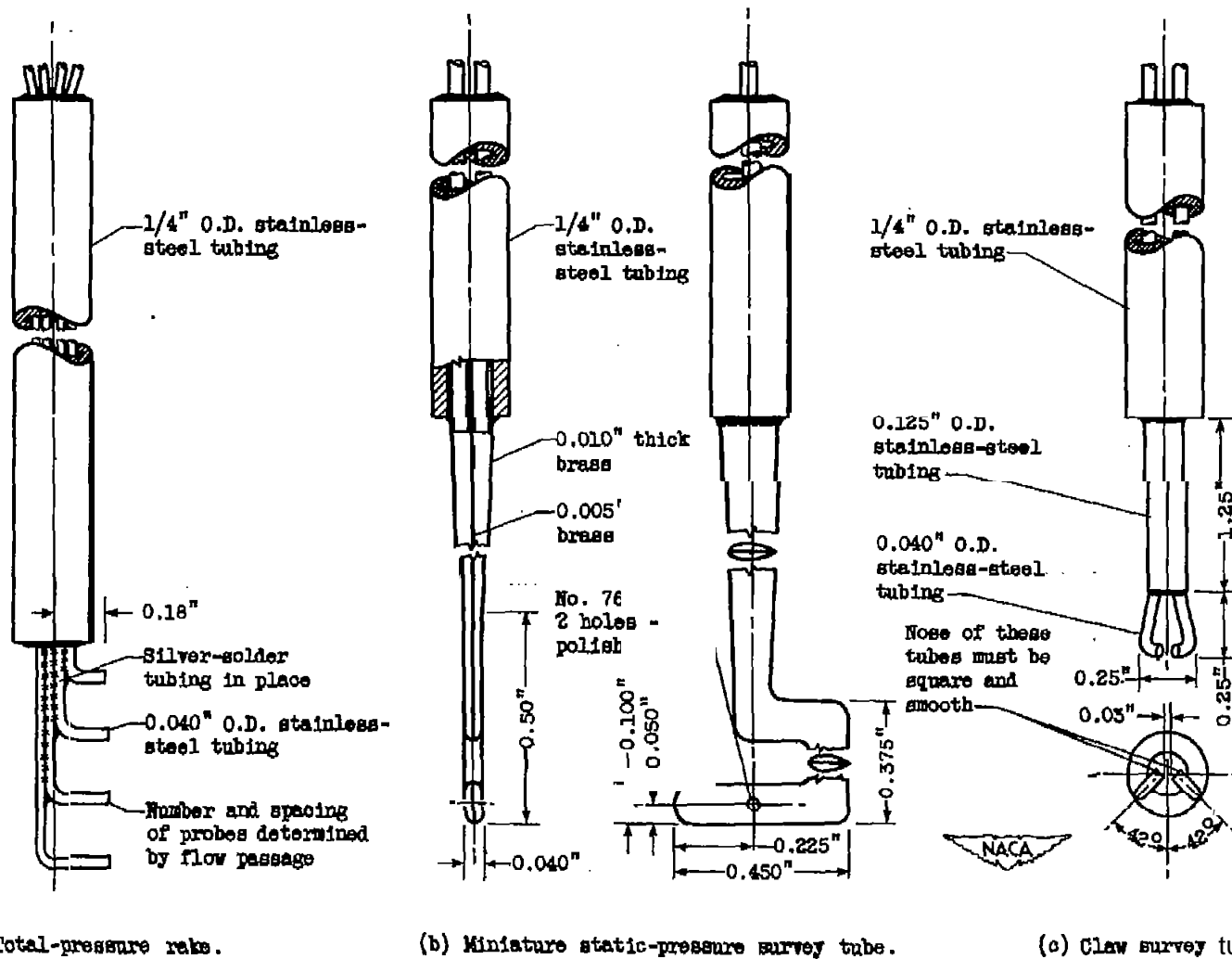


Figure 2. - Experimental setup for single-stage axial-flow compressor.



(a) Total-pressure rake.

(b) Miniature static-pressure survey tube.

(c) Claw survey tube.

Figure 3. - Instruments used in compressor-performance investigation.

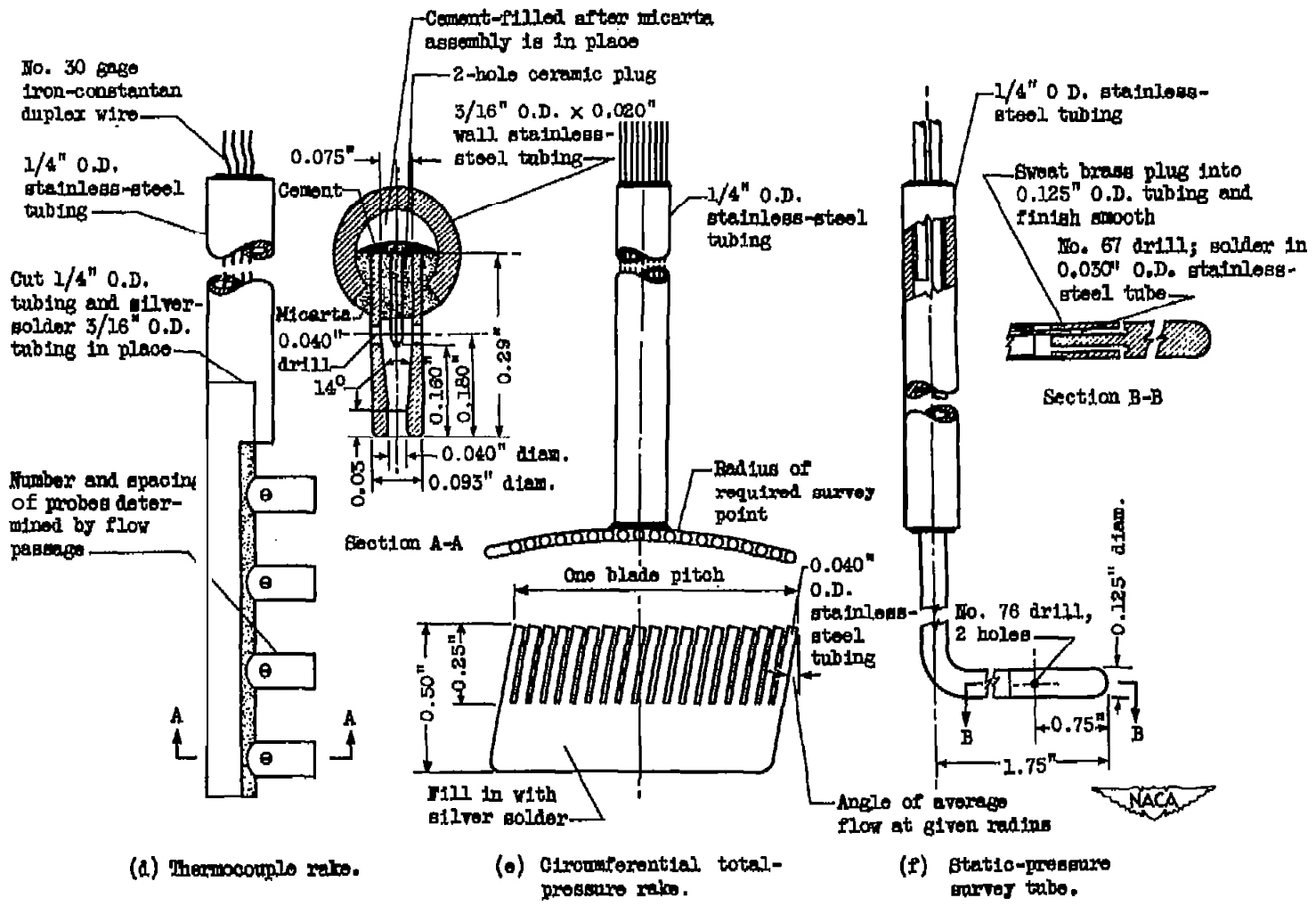


Figure 3. - Concluded. Instruments used in compressor-performance investigation.

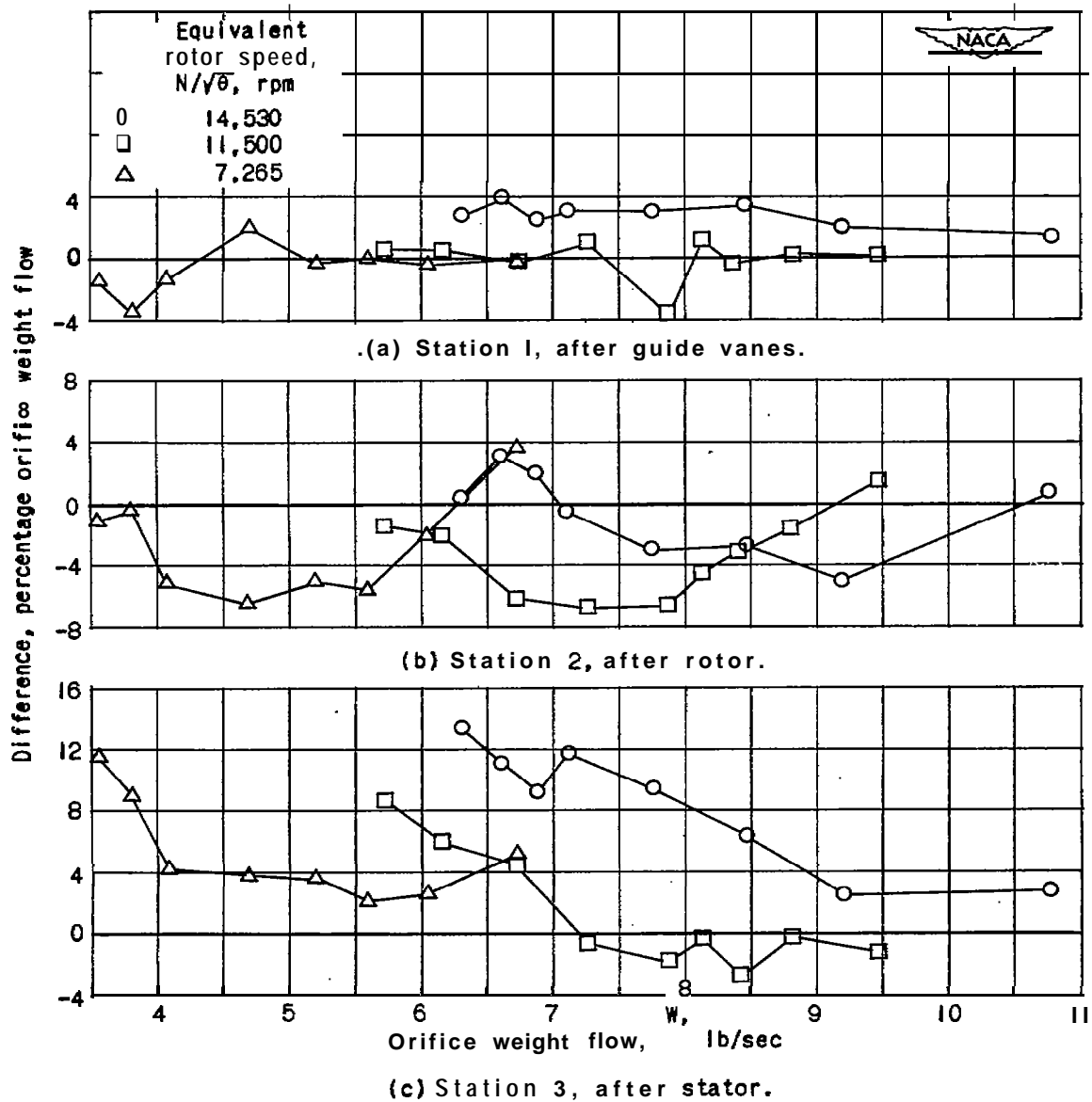


Figure 4. - Difference between integrated weight flows at three measuring stations and orifice weight flow expressed in percentage of orifice weight flow.

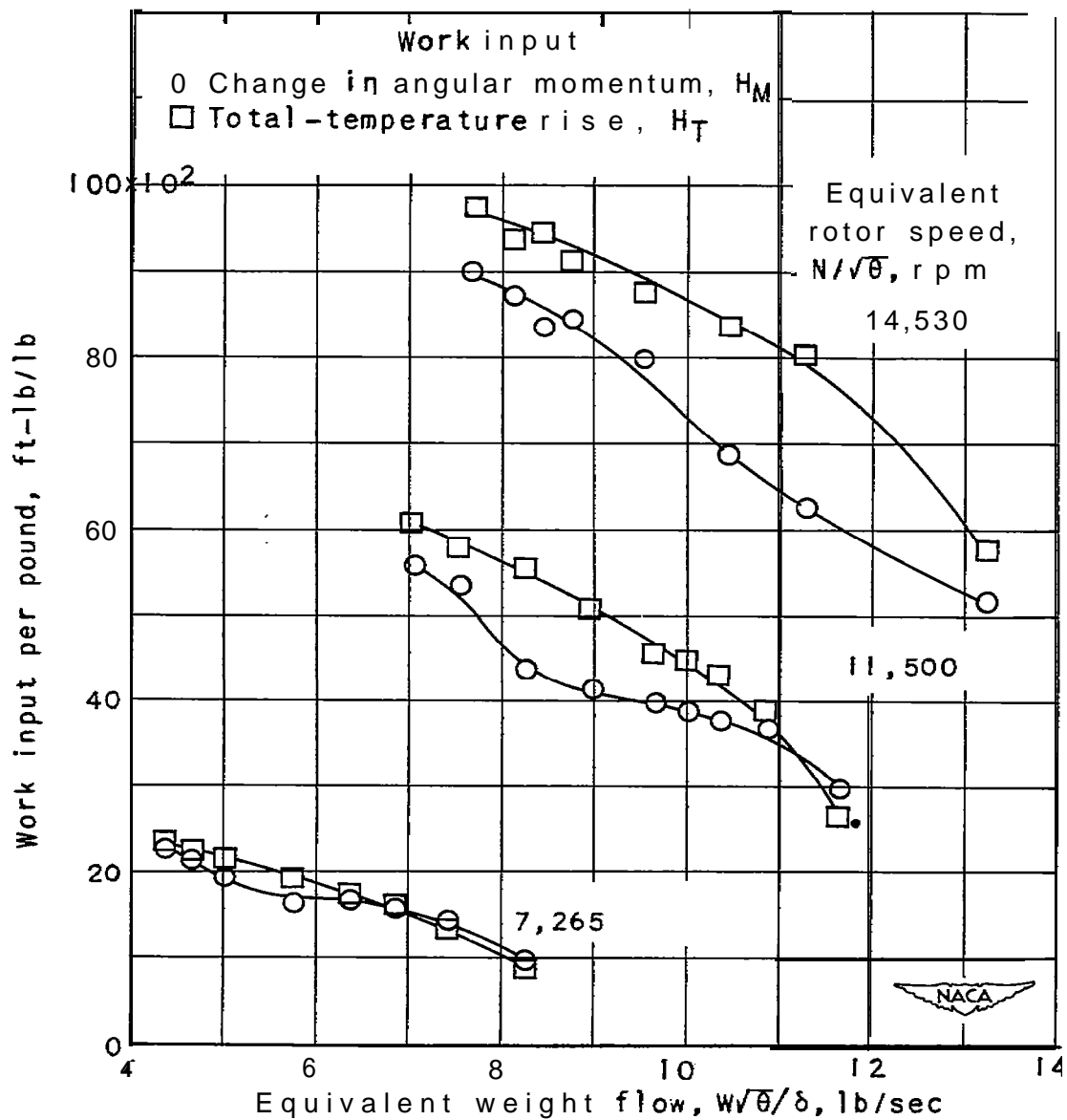


Figure 5. - Comparison of two methods of measuring work input to air.

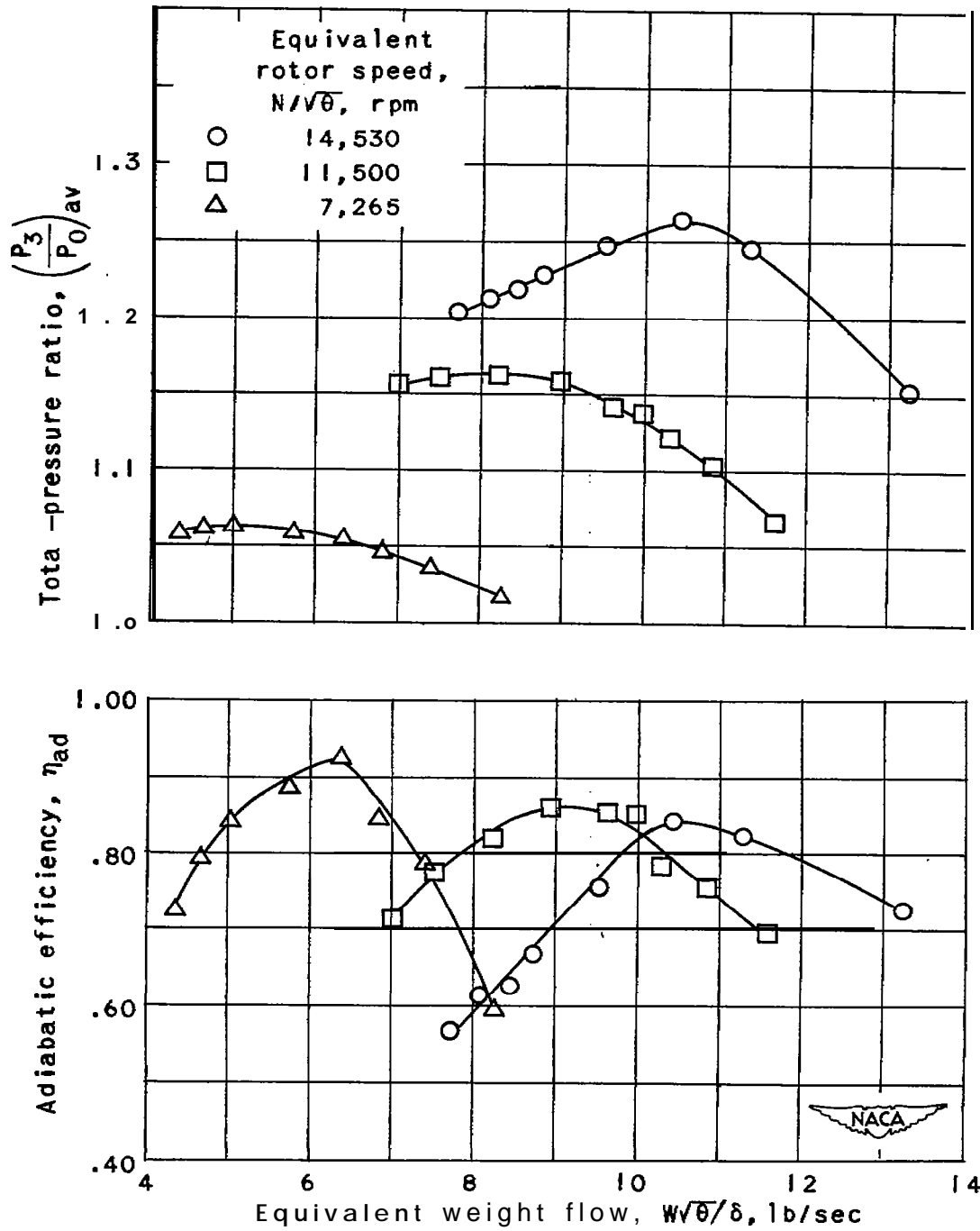
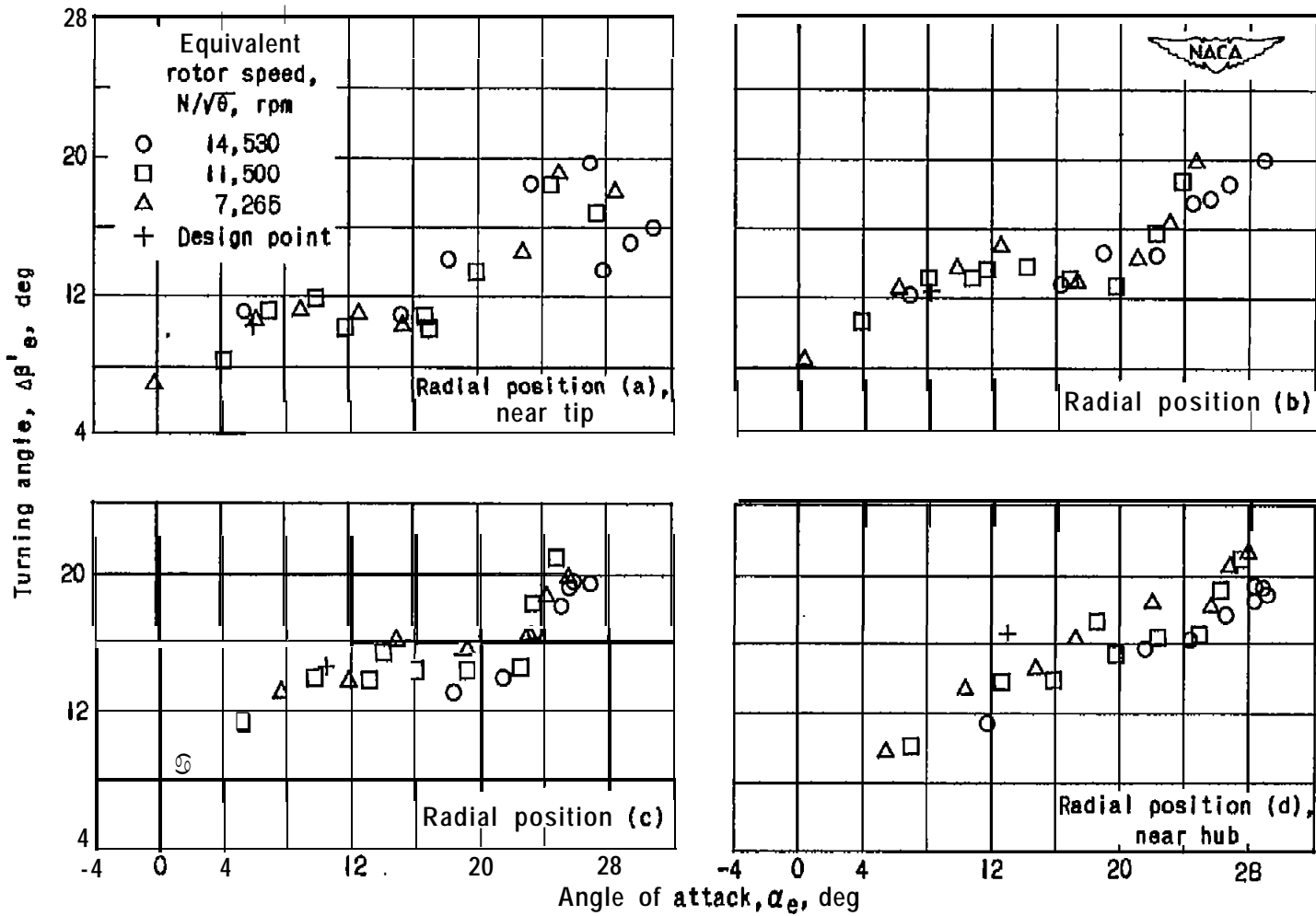
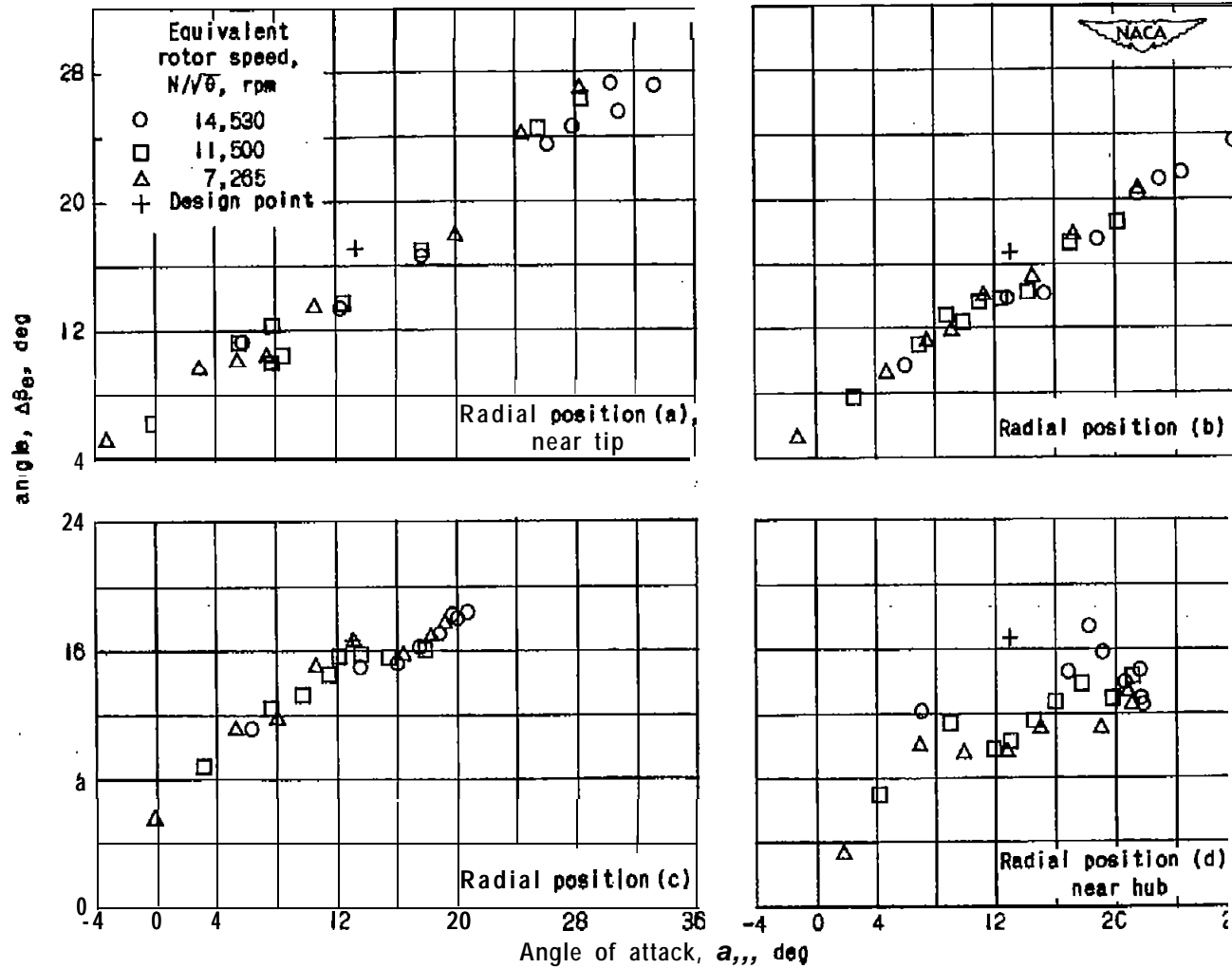


Figure 6. - Over-all performance of a 14-inch diameter single-stage axial-flow compressor using the NACA 5509-34 blade section.



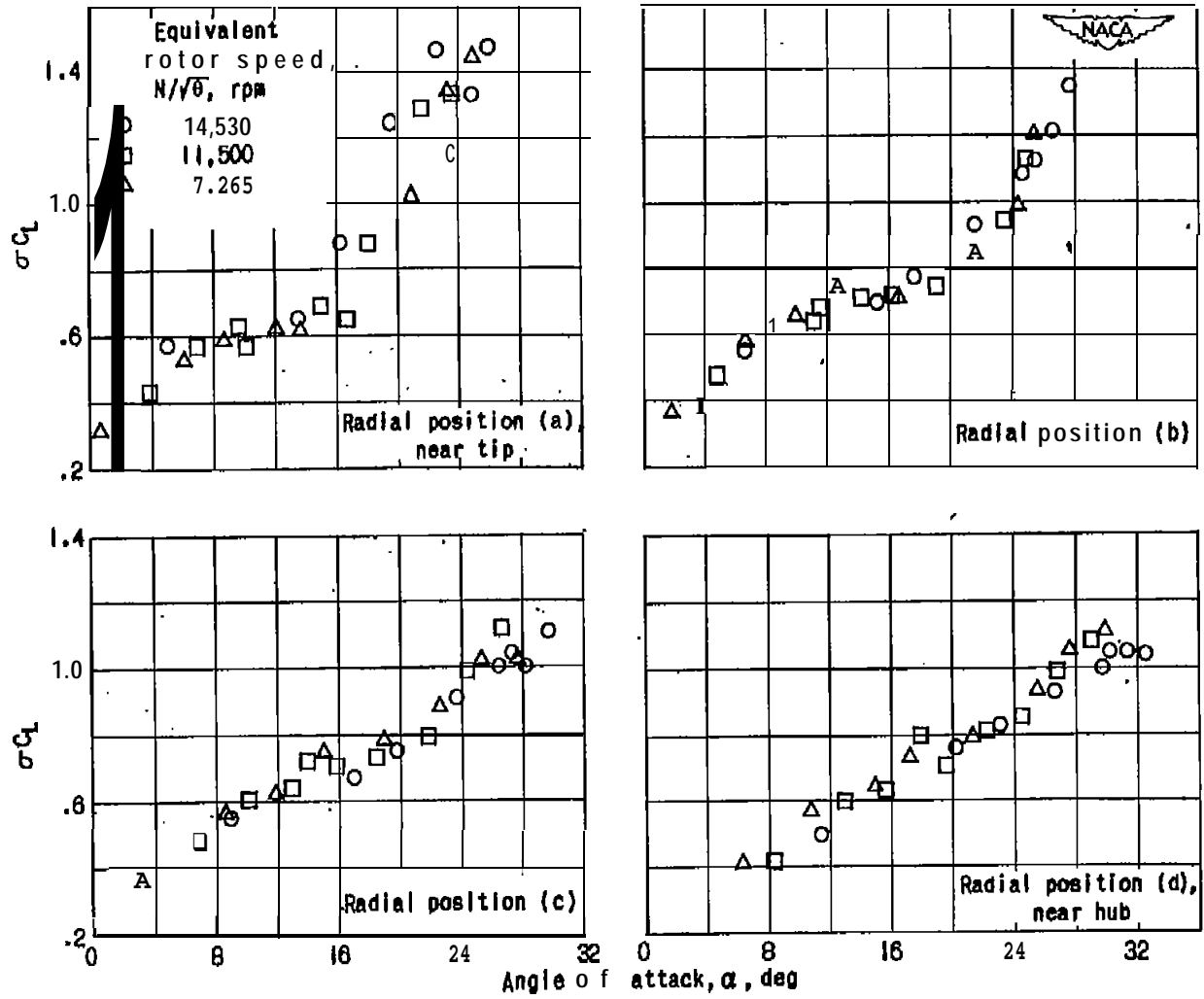
(a) Rotor.

Figure 7. - Variation of turning angle $\Delta\beta'_e$ with angle of attack α_e . NACA 5509-34 blade section.



(b) Stator.

Figure 7. - Concluded. Variation of turning angle $\Delta\beta_e$ with angle of attack α_e . NACA 55W-34 blade section.



(a) Rotor.

Figure 8. - Variation of σC_L with angle of attack α . NACA 5509-34 blade section.

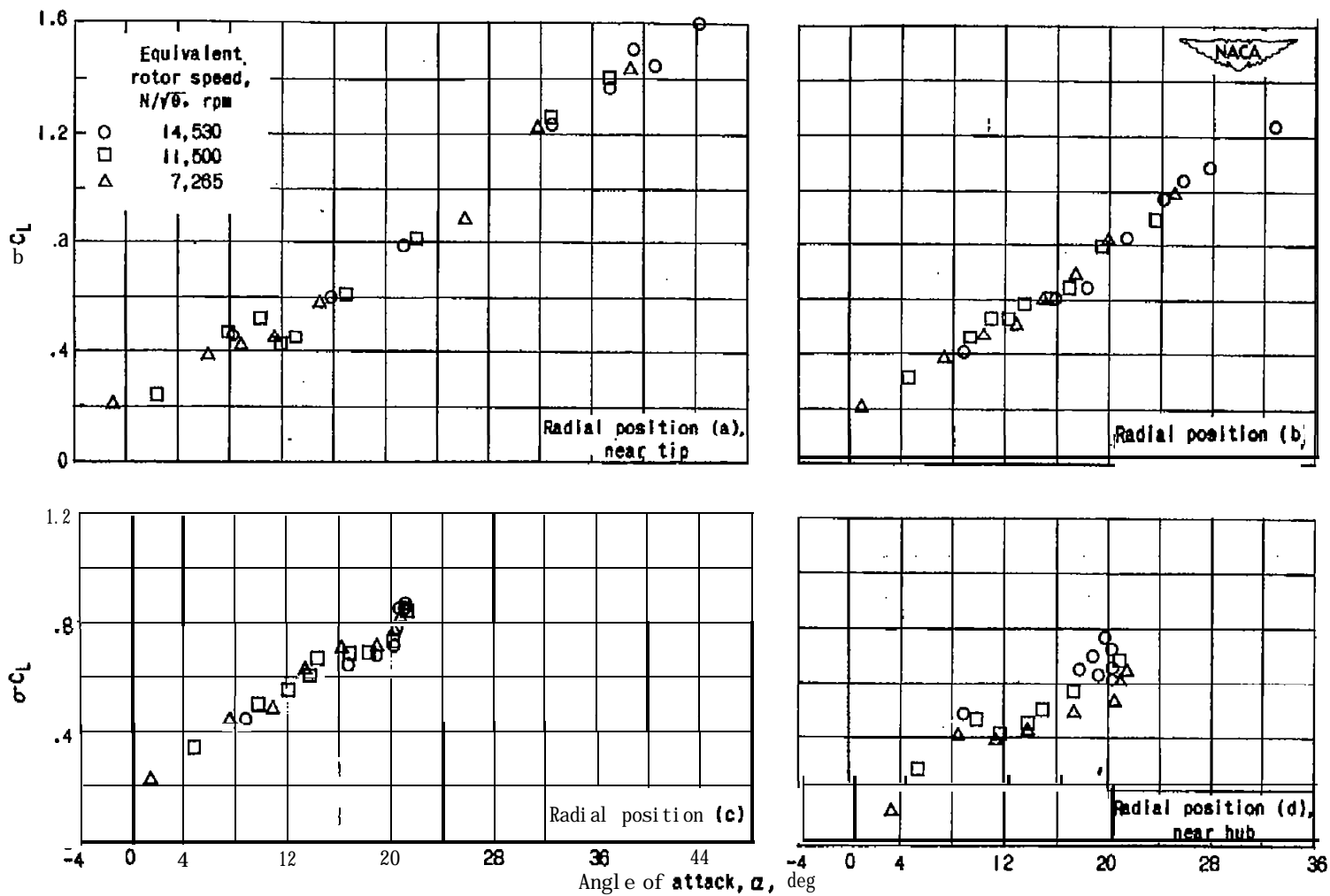
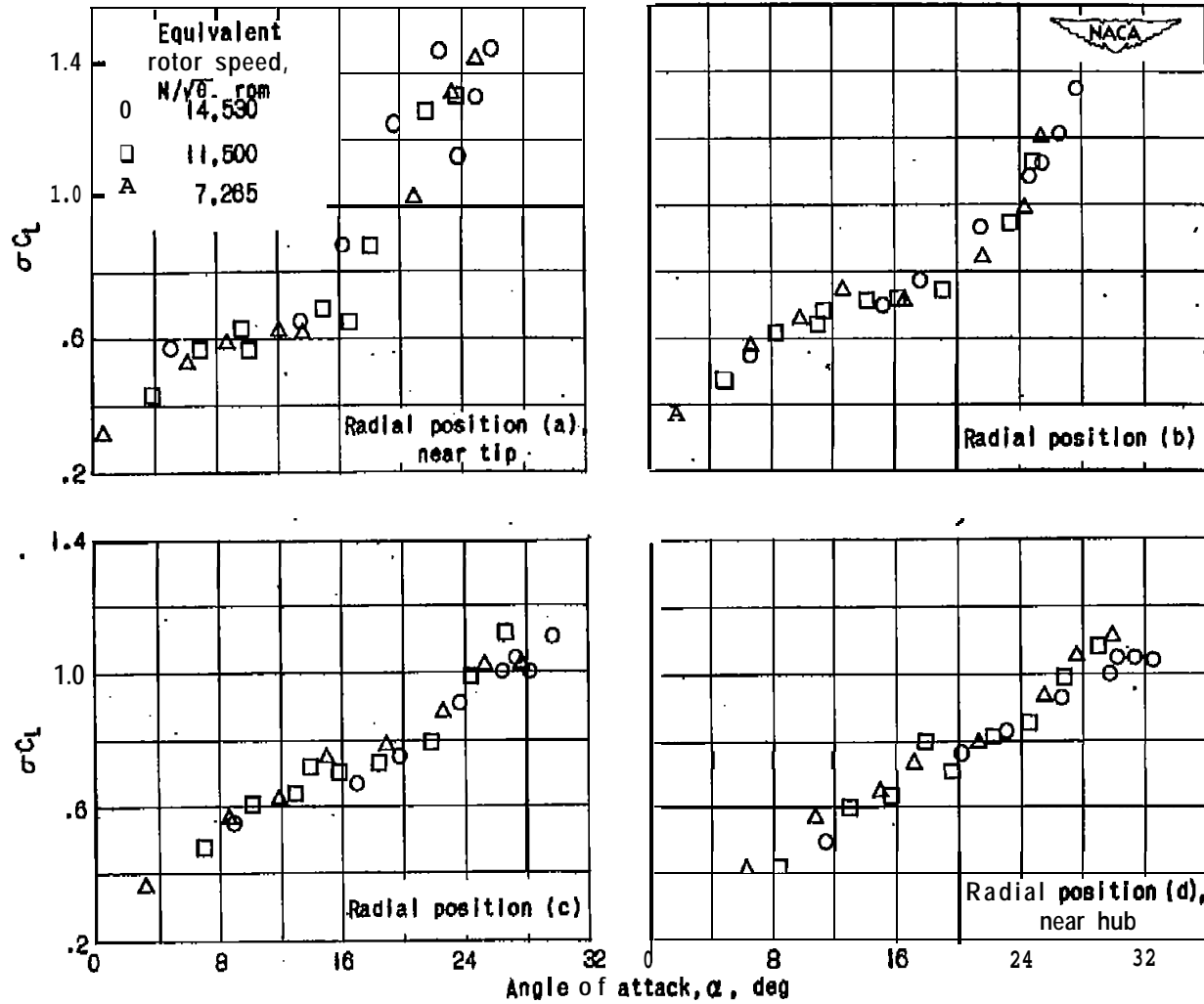
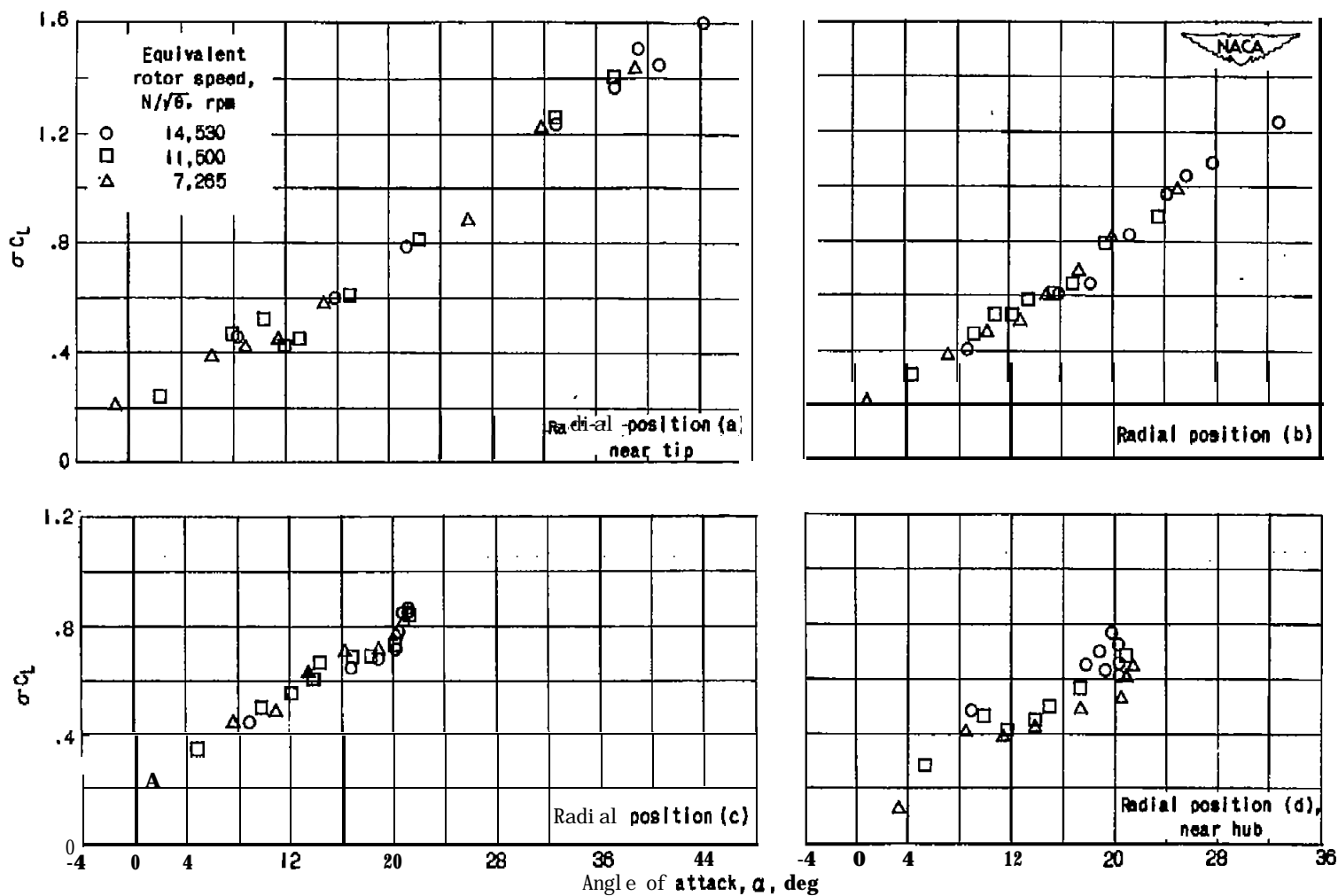


Figure a. - Concluded. Variation of σC_L with angle of attack α . NACA 5509-34 Blade section.



(a) Rotor.

Figure 8. -Variation of σC_L with angle of attack α . NACA 5509-34 blade section.



(b) Stator.

Figure a. - Concluded. Variation of σC_L with angle of attack. NACA 5509-34 blade section.

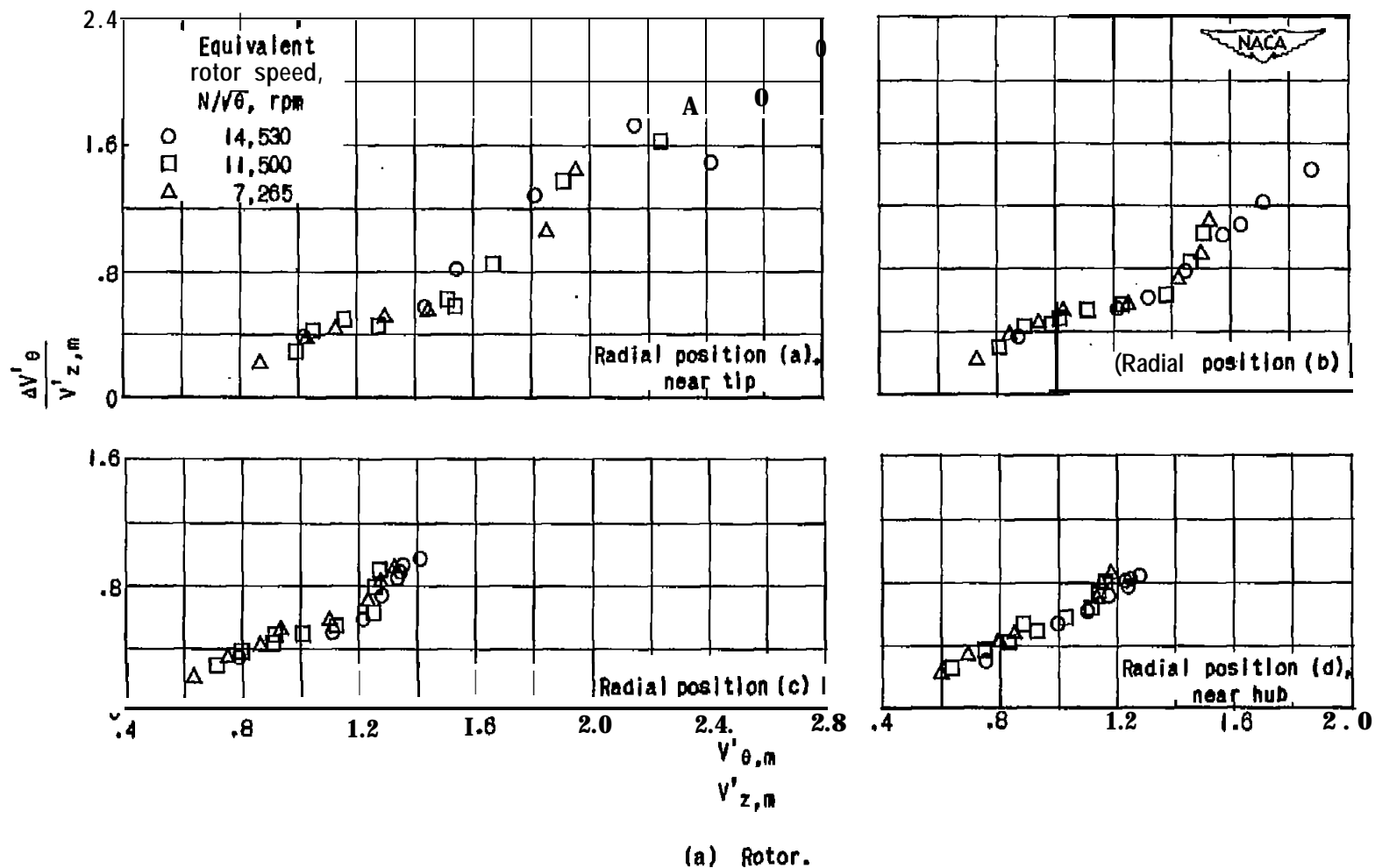
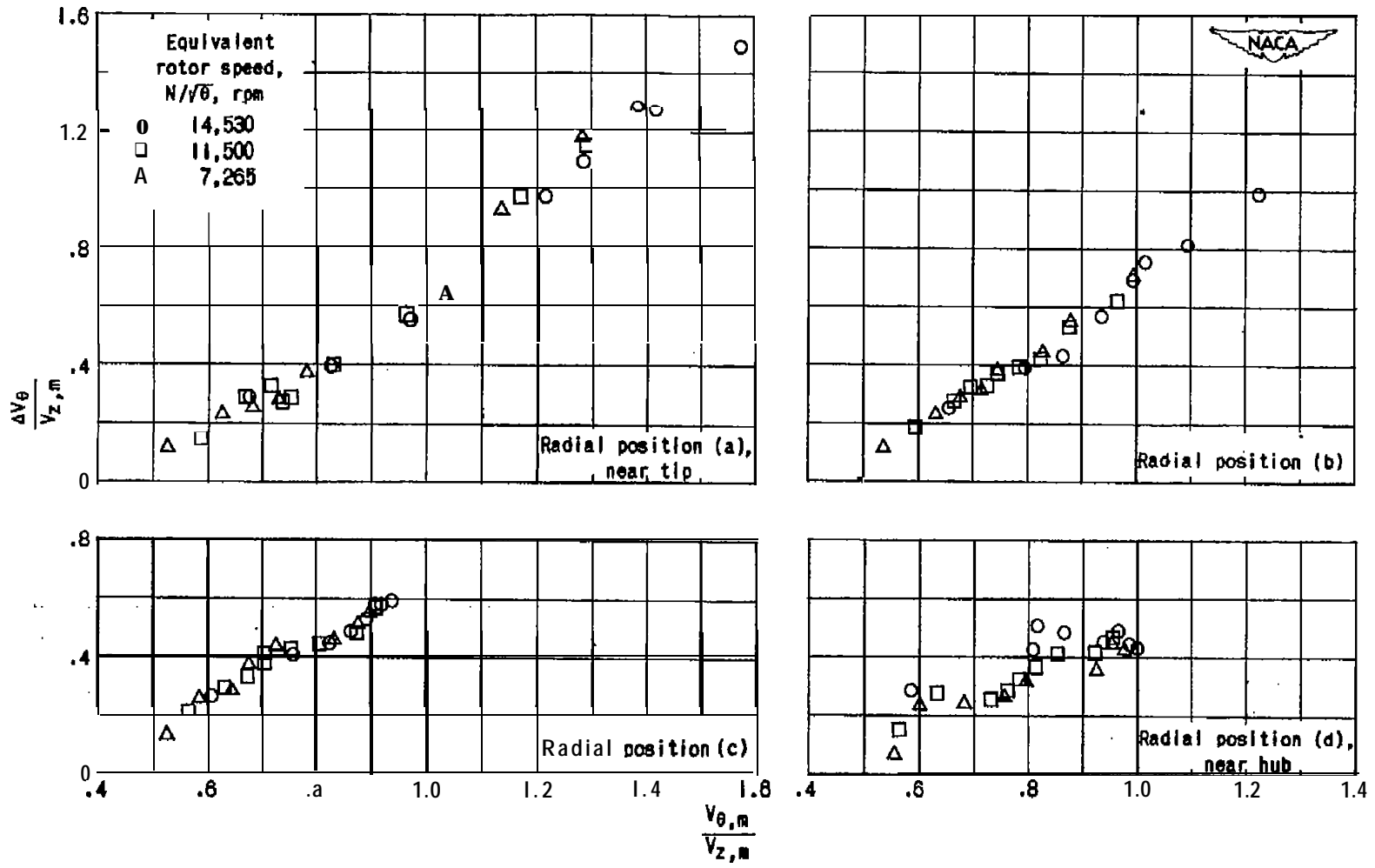


Figure Q. - Variation of blade-loading parameter $\Delta V'_{\theta}/V'_{z,m}$ with $V'_{\theta,m}/V'_{z,m}$. NACA 5509-34 blade section.



(b) Stator.

Figure Q. -Concluded. Variation of blade-loading parameter $\Delta V_{\theta}/V_{z,m}$ with $V_{\theta,m}/V_{z,m}$. NACA 5500-84 blade section.

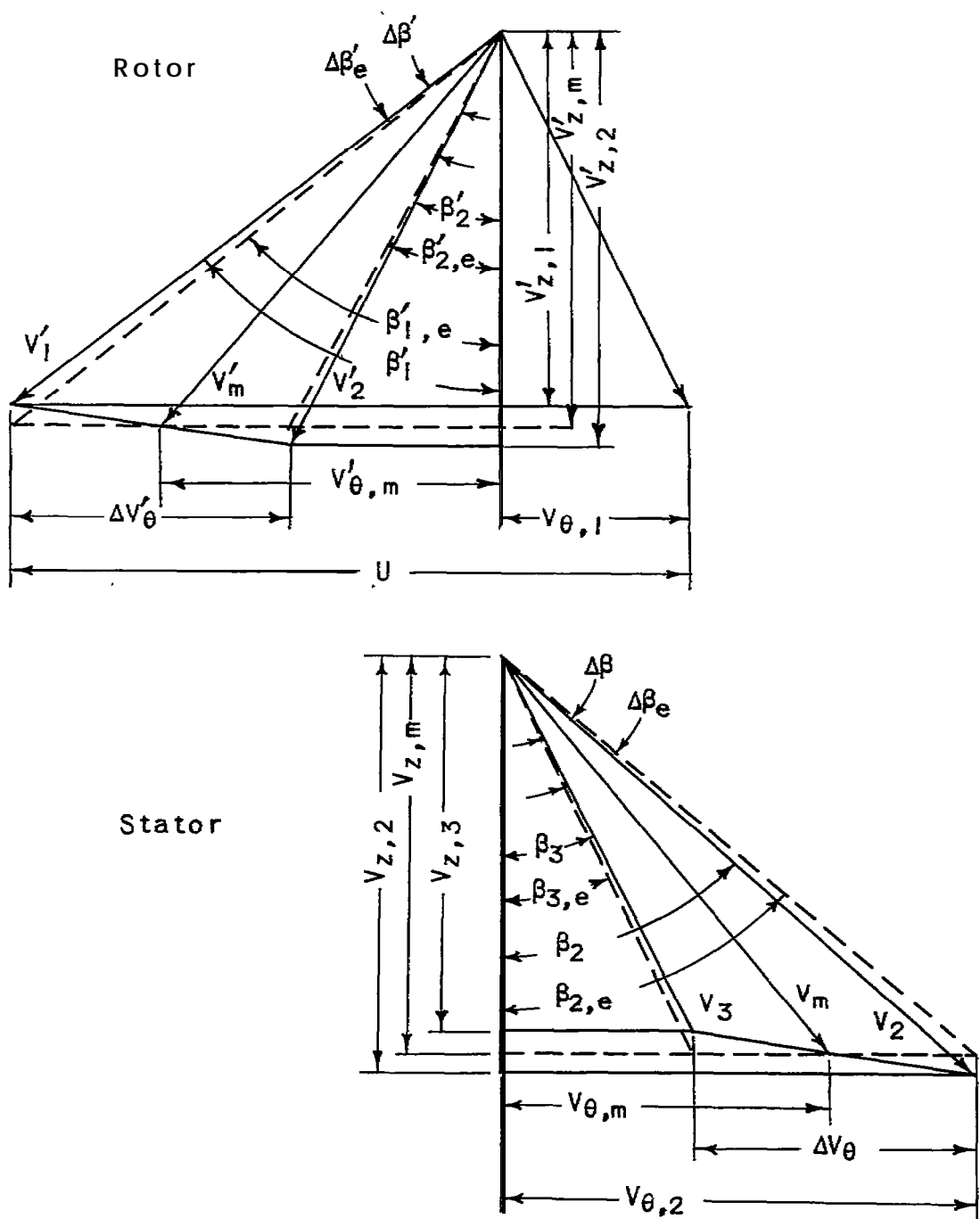


Figure f 0. - Typical velocity diagram for single-stage axial-flow compressor.

NASA Technical Library



3 1176 01435 5441